Adaptive Polynomial Predistorters and low-PAR circular APK Signaling Schemes for Systems Using Non-linear Power Amplifiers

Thai Hoa Vo

A Thesis
in
The Department
of
Electrical and Computer Engineering

Presented in Partial Fulfilment of the Requirements
for the Degree of Master of Applied Science at
Concordia University
Montreal, Quebec, Canada

November, 2002

Your file Votre référence
ISBN: 0-612-83966-4
Our file Notre référence
ISBN: 0-612-83966-4

Abstract

Adaptive Polynomial Predistorters and low-PAR circular APK Signaling Schemes for Systems Using Non-linear Power Amplifiers

Thai Hoa Vo

In this thesis, adaptive polynomial predistortion techniques suitable for DSP implementation at the baseband signals are introduced to counter-balance the AM/AM and AM/PM nonlinear effects of the transmit power amplifier. The proposed polynomial predistortion scheme is based on polar coordinate representation. Both LMS and RLS concepts are used to derive the adaptive algorithms. An enhanced LMS-based algorithm with fast convergence is proposed. For very fast convergence, a cascaded RLS-based adaptive polynomial predistorter structure is introduced. The obtained results show that the polynomial predistortion schemes can be used in M-QAM transmitters with power amplifiers operating near saturation to achieve a highest power efficiency. The thesis also presents a class of circular M-ary Amplitude-Phase Shift Keying (APK) signaling techniques with high bandwidth efficiency and low peak-to-average power ratio (PAR) suitable for systems using non-linear power amplifiers to achieve high power efficiency. Based on bandlimited two-dimensional M-ary signals using circular constellations, a search algorithm for optimum schemes for non-linear amplification in terms of minimum PAR and maximum DPR is introduced. Optimum circular constellations for 8-, 16-, 32-, 64- and 128-APK signalling schemes are proposed. The analytical and simulation results show that this class of circular M-ary APK signals outperforms the square and cross M-ary QAM schemes.

Acknowledgments

I would like to express my sincere gratitude to my supervisor, Professor Tho Le-Ngoc for his invaluable guidance, encouragement and support throughout the course of my thesis work. He contributed a great deal of his time, efforts and ideas to the work presented in this dissertation. I am grateful that he is an advisor who always provided options rather than decisions.

I would like to thank CITR in funding this project. Special thanks to Dr. Hichem Besbes for his valuable advice and suggestions on the LMS algorithms. I also would like to thank Dr. Champagne and Dr. Shayan for their constructive suggestions and comments to improve the thesis.

I would like to take this opportunity to mention the tremendous supports in every day life that I have received from my parents, brother and sisters. I also would like to thank my uncle, Bach, who has always encouraged and motivated me to pursue the graduate study. Finally, I am very appreciative for the patient, love and support from my fiancee, Q. Giao, during my graduate study.

Table of Contents

List of Figures

List of Tables

Acronyms

AM-AM	Amplitude to amplitude
AM-PM	Amplitude to phase
APK	Amplitude phase shift keying
ASIC	Application specific integrated circuit
ASK	Amplitude shift keying
AWGW	Additive white Gaussian noise
CALLUM	Combined analogue locked loop universal modulator
CPFSK	Continuous phase frequency shift keying
DPR	Squared minimum distance to average power
DSP	Digital signal processing
FM	Frequency modulation
HPA	High power amplifier
IIP3	Input power at third order intercept point
IM	Intermodulation
IMD	Intermodulation distortion
IM3	Third order intermodulation product
IP3	Third order intercept point
LINC	Linear amplification with nonlinear components
LMS	Least mean square
MSE	Mean square error
OBE	Out of band emission
OBO	Output backoff power
OIP3	Output power at third order intercept point
PAM	Pulse amplitude modulation
PAR	Peak to average power ratio
PBO	Peak backoff power
PSD	Power spectrum density
PSK	Phase shift keying

QAM	Quadrature amplitude modulation
QPSK	Quadrature phase shift keying
RF	Radio frequency
RLS	Recursive least square
SER	Symbol error rate
SNR	Signal to noise ratio
SRRC	Square root raised cosine
SSPA	Solid state power amplifier
TD	Total degradation

Chapter 1. Introduction

M-QAM has been considered to achieve high bandwidth efficiency for broadband wireless communications. However, due to its envelope fluctuation, it exhibits large spectral re-growth causing performance degradation when the transmit high power amplifier (HPA) operates in a nonlinear region close to saturation in order to achieve the high power efficiency. High power efficiency helps in reducing power consumption, which is important and desired in many applications, especially in the case of portable systems using battery.

The nonlinear characteristics of a transmit high power amplifier (HPA) can be represented by their AM/AM and AM/PM effects, which indicate the non-linear relationships between the output amplitude/phase-shift and input amplitude (or power). Therefore, a modulated signal with a large envelope variation such as filtered M-QAM suffers both amplitude and phase distortions when it is non-linearly amplified. As results of these distortions, the receiver performance in terms of bit error rate will be degraded, and the spectrum of transmitted signal will be spread to adjacent channels, causing adjacent-channel interference. One approach to avoid this problem is to operate the HPA at a large output backoff from its saturated power, in order to maintain the required linearity at the expense of reduction in power efficiency.

Several HPA linearisation techniques have been proposed in order to achieve high spectral and power efficiency. These techniques can be classified in three categories [1]: i) Feed-Forward [2], ii) Cartesian Feedback [3] and iii) Predistortion.

Feed-forward linearizer uses two amplifiers. It is designed with the aim to have the distortion of these amplifiers perfectly cancel each other. However, it can not be controlled against the effects of HPA parameters variation due to the temperature,

component aging,... A rigorous analysis of adaptation behavior of a feed-forward linearizer is presented in [4].

In [3] HPA linearisation by Cartesian feedback has been analyzed using a multiple input multiple output model. It was shown that the Cartesian feedback can suffer from stability depending on HPA nonlinearity characteristics and stability margin.

Predistortion techniques have been proposed as a potential solution to overcome the non-linear distortion effects [5,6]. Basically, these techniques aim to introduce "inverse" nonlinearities that can compensate the AM/AM and AM/PM distortions generated by the nonlinear amplifier. In general, a predistorter can be implemented using analog or digital circuitry. Namiki [7] introduced a simple automatic control technique for third-order analog predistorter. However, digital predistorters have become more popular due to their easy implementation and design. Two sub-categories of predistortion techniques have been proposed depending on where the predistortion process is inserted. The first one is based on pre-distorting the signal constellation in such a way that the distortion introduced by the combination of the HPA nonlinearity and the channel memory is cancelled [8,9,10]. This approach can be realized by various techniques, e.g., Volterra series [11], artificial neural network [12], p^{th}-order inverse of a Volterra series [13], Hammerstein model for the predistorter [14]. These techniques require high computational complexity and their convergence rate and steady-state performance depend on the transmitted alphabet size. The second one uses a memoryless nonlinear device placed between the shaping filter and the HPA. This nonlinear device can be designed digitally using a mapping predistorter (with a look-up table) or a polynomial function in Cartesian or polar representation. Nagata [6] has presented a two-dimensional table look-up technique with adaptive digital feedback at baseband. This technique has the advantage to perform any order of the non-linearity and any modulation technique. Cavers [15,16,17] and Faulkner and Johansson [18] proposed one-dimensional table look-up techniques with very promising results in Cartesian and polar representations, respectively.

Several adaptive complex polynomial predistorters were proposed [19,20,21,22] with the main objectives to increase the convergence rate and to reduce the complexity. In

[20], the predistorter polynomial coefficients are derived for minimum out-of-band inter-modulation distortion (IMD). The third, fifth, and possibly seventh order components can be suppressed, thus the optimization process does not guarantee the convergence to the global minimum. In [21, 22], the authors proposed to adapt the predistorter coefficients by using a post-distorter with an RLS algorithm. The presented simulation results promise a distortion suppression of 45dB. However, this technique has a higher complexity as compared to the previous solution. An evaluation of a predistortion technique should take into account both its performance and complexity. Moreover, to achieve a better performance, a higher sampling rate is preferred, and consequently, low-complexity adaptive method is suggested [23].

In this thesis, we propose adaptive polynomial predistortion techniques in polar representation and both LMS and RLS concepts. An enhanced LMS-based adaptive polynomial predistorter algorithm with low complexity and fast convergence is introduced. For applications requiring a very fast convergence, we develop the RLS-based adaptive polynomial predistorter structures with relatively low complexity (e.g., lower than the one in [22]). The proposed predistortion techniques show that M-QAM signaling can be used with a transmit power amplifier operating near saturation to achieve a highest power efficiency, while its transmitted spectrum and performance are maintained close to those in a linear channel. The convergence behavior of the adaptive predistortion technique is analyzed. The spectral regrowth and performance of 16 and 64QAM system using a pre-distorter/HPA are evaluated using simulations. The effects of polynomial order, quantization noise, and HPA parameter variations are studied.

With the use of HPA linearisation, several results reported in [15, 18, 24] indicate that systems can operate with the *peak* power extremely close to the HPA saturation. Therefore, a modulated signal with low *peak-to-average power ratio* (PAR) is desired to increase the power efficiency. For bandlimited (modulated) signals, the PAR is contributed by the filtering and the constellation. On the other hand, signals with high *squared minimum distance to average power ratio* (DPR) will provide the best error performance. Hence, it is desired to have a constellation with small PAR and high DPR.

Based on bandlimited two-dimensional M-ary signals using circular constellations, we develop a search algorithm for optimum schemes for non-linear amplification in terms of minimum PAR and maximum DPR and find the optimum circular constellations for 8-, 16-, 32-, 64- and 128-APK signalling schemes. The effects of bandlimiting filter sharpness on the PAR are examined and considered in the development.

The thesis is organized as follows. Chapter 2 presents the background. Chapter 3 describes the proposed predistorter structure and discusses its steady-state performances. Chapter 4 presents the proposed adaptive algorithms based on both LMS and RLS concepts and examines their behavior. Chapter 5 discusses the optimum circular APK constellations and the proposed algorithm for seaching these constellations. Conclusions are given in Chapter 6.

Chapter 2. Power Amplifier Non-linear Characteristics and Linearization/Predistortion Techniques

2.1 Bandwidth-efficient Multilevel Modulation and Transmission

Figure 2.1 depicts a basic block diagram of a transmitter.

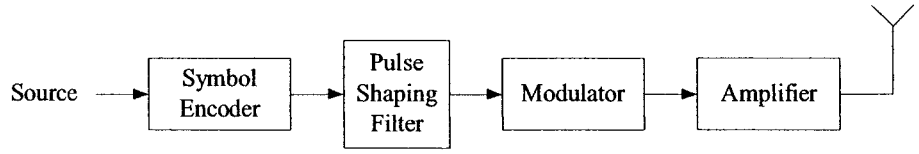

Fig. 2.1: Basic block diagram of a transmitter

The source is a sequence of bit, which is converted to a sequence of symbols by the symbol encoder. The symbol encoder operates at the rate of $f_{sym} = 1/T_{sym}$, where T_{sym} is the duration of a symbol. Each symbol is taken from an alphabet of M possible elements, where M is often chosen that $M = 2^k$, and k is the number of bits per symbol. For bandwidth-efficient modulation schemes, higher spectrum efficiency can be achieved by increasing k, at the expense of an increase in signal-to-noise ratio to maintain the same performance. The symbol encoder is sometimes referred as vector modulation, because it maps a group of k bits to a symbol vector in a L-dimensional space. When L=1, it is equivalent to PAM for baseband transmission or ASK for passband transmission. The value of L equals to 2 is widely used in many practical systems. A

symbol is denoted by a point (I_n, Q_n) in a 2 dimensional space made up by the in-phase and quadrature-phase axis. A signal is then filtered and modulated to a specific carrier frequency f_c. The modulated signal is amplified to a required power level before being delivered to the channel via an antenna.

In general, a modulated signal can be represented as,

$$x(t) = A(t)\cos(2\pi f_c t + \phi(t)) \tag{2.1}$$

where f_c is the carrier frequency. The bandwidth of the phase function $\phi(t)$ and the amplitude function $A(t)$ are in general much lower than the carrier frequency f_c. Note that the occurrence of the functions $A(t)$ and $\phi(t)$ in the equation 2.1 implies that $x(t)$ can represent both amplitude or/and phase modulation techniques. Consequently, $x(t)$ is a passband signal with its spectrum concentrated around the carrier frequency f_c. The signal $x(t)$ can be rewritten as,

$$x(t) = x_I(t)\cos(2\pi f_c t) + x_Q(t)\sin(2\pi f_c t) \tag{2.2}$$

where

$$x_I(t) = A(t)\cos(\phi(t))$$

$$x_Q(t) = -A(t)\sin(\phi(t))$$

represents the quadrature components. $x_I(t)$ is the in-phase (I) and $x_Q(t)$ is the quadrature-phase (Q) components. A simple way to generate RF signal is shown in Figure 2.2.

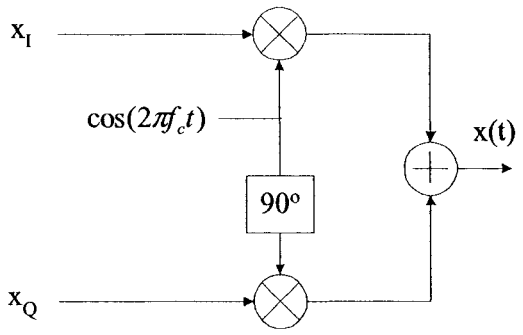

Fig. 2.2: Modulator block

The in-phase and quadrature-phase components are affected by both amplitude and phase functions. If the amplitude is constant and the phase varies, it is called M-ary PSK (Phase Shift Keying) modulation technique. For fixed phase and varying amplitude, the result will produce a M-ary ASK (Amplitude Shift Keying) modulation. When both amplitude and phase are changed, it will form a M-ary APK modulation technique. Quadrature Amplitude Modulation (QAM) is a special case of ASK where the in-phase and quadrature-phase components are PAM signals. Some typical constellations of different modulation schemes are shown in the figures 2.3 and 2.4.

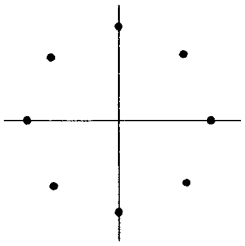

Fig. 2.3: 8-PSK constellation

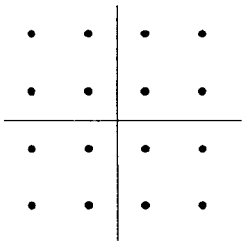

Fig. 2.4: 16-QAM constellation

For bandlimited QAM modulation, the root raised cosine (RRCS) filter is often used for spectrum shaping. In a linear channel with RRCS used in the receiver, zero intersymbol interference (ISI) and optimum symbol-by-symbol detection in an additive white Gaussian noise (AWGN) environment are achieved [25]. The rolloff factor of the RRCS controls the occupied bandwidth of the transmitted signal. It is noticed that QAM signal has a varying envelope due to transitions from one signaling element to another.

For example, there are 180-degree transition trajectories in 4-QAM (QPSK) shown in Figure 2.5 representing 100% amplitude modulation. Large amplitude variation introduces both amplitude and phase distortions when the modulated signal passes through a non-linear amplifier.

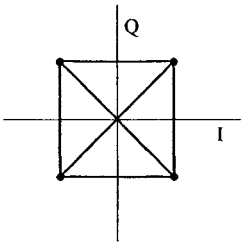

Fig. 2.5: Transition trajectories of 4-QAM (QPSK)

2.2 Power Amplifier Characteristics

The efficiency of a power amplifier can be represented by the ratio of the operating RF transmitted power to the DC supply power. In general, based on the design approaches, power amplifiers can be classified into four general classes: A, B, AB, and C [26]. Class-B, AB, and C power amplifiers operate in a non-linear manner to achieve high power efficiency. They are applicable to constant-envelope modulated signals such as FM, CPFSK. For multilevel APK and QAM, Class-A power amplifiers are often used for QAM to achieve the required linearity at the expense of reduced power efficiency.

The input-output relationship of a class-A power amplifier is only linear for a small range. As the input amplitude signal increases, the input-output relationship is no longer linear and its nonlinear characteristics cause distortions in the modulated signal, leading to performance degradation and further reduce the power efficiency. In the following sub-sections, we will discuss the characteristics of the class-A power amplifiers and their effects.

2.2.1 Input-output relationship and relevant parameters:

Figure 2.6 shows the typical input-output power relationship of a class-A power

amplifier with the input and output power presented in dBm or dBW. The dashed line with slope of 1 represents the *ideal* linear relationship, i.e.,

$$\textit{output}\ \text{signal power}_{[\text{in dBm}]} = \textit{input}\ \text{signal power}_{[\text{in dBm}]} + \text{power gain}_{[\text{in dB}]}$$

The *ideal* linear relationship is close to the *actual* input-output power relationship for a certain range of small input power. Howerver, beyond this range, the relationship becomes *non-linear* with *reduced* output power. The *1-dB compression point* is defined as the point at which the actual output power is reduced by 1dB as compared to the *expected* value of the *ideal* linear relationship. As the input power continues to increase beyond the 1-dB compression point, the output power slowly increases and reaches the *saturation point*, indicating the maximum possible RF output power. The input power corresponding to this point is called the *saturated input power* and the output power is called the *saturated output power.* After this point, the output power will always remain equal or less than the saturated output power with increased input power.

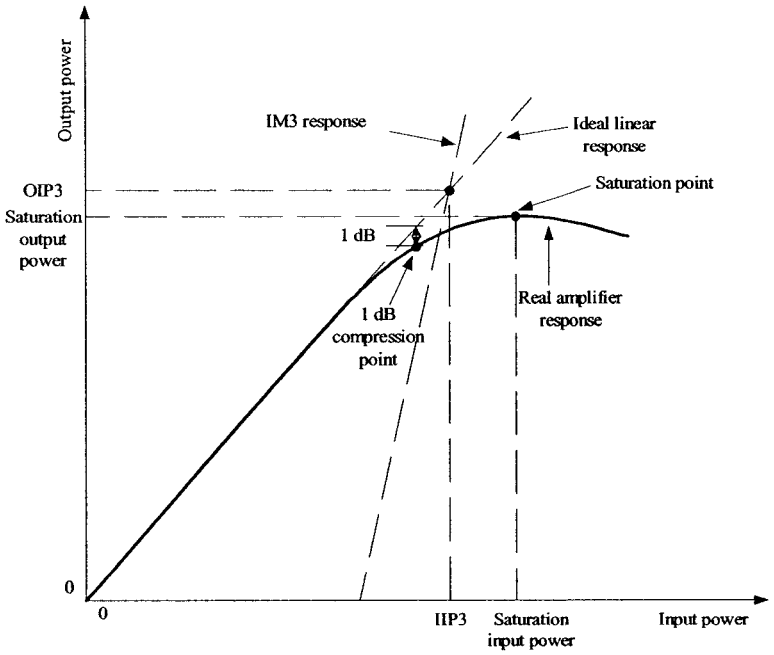

Fig. 2.6: Typical Input-Output Relationship of a Power Amplifier

The nonlinear input-ouput relationship of a memoryless power amplifier can be

expressed as a power series,

$$s_o(t) = c_0 + c_1 s_i(t) + c_2 s_i^2(t) + c_3 s_i^3(t) + \ldots \tag{2.3}$$

where $c_o, c_1, c_2, \ldots$ are real value coefficient. $s_i(t)$, $s_o(t)$ are the instantaneous input and output amplitudes at the time t.

When a single-carrier signal with a fundamental frequency f_c is applied to the input, the corresponding output contains a number of carriers at harmonic frequencies nf_c. These harmonic frequencies are undesirable to the system. However, they are out of the frequency band of interest and can be eliminated by bandpass filtering.

The distortion in the desired output signal of a power amplifier can be observed by substituting the single-tone input signal $s_i(t) = a_i \cos(2\pi f_c t + \phi_i)$ into Equation (2.3). The output tone at the fundamental frequency is,

$$s_{1o}(t) = \left(c_1 a_i + \frac{3c_3 a_i^3}{4} + \frac{5c_5 a_i^5}{8} + \ldots \right) \cos(2\pi f_c t + \phi_i) \tag{2.4}$$

The above equation indicates that only the odd coefficients contribute to the distortion of the amplifier output.

The above equation only represents the amplitude distortion of the signal output of a power amplifier. The signal output phase also varies and depends on the input amplitude. This amplitude-to-amplitude (AM-AM) and amplitude-to-phase (AM-PM) distortion will be discussed in detail in the next chapter.

If the input is the sum of two tones at the frequencies $f_1 = f_c - f_m$ and $f_2 = f_c + f_m$ then the output of power amplifier contains the the two fundamental tones, their harmonics at mf_1 and nf_2, and tones at $kf_1 \pm pf_2$ (called *intermodulation products*) as shown in Figure 2.7. The intermodulation (IM) products are in the band of interest and hence cannot be easily eliminated by filtering. The closest IM products are the third-order ones at frequencies $2f_1 - f_2 = (f_c - 3f_m)$ and $2f_2 - f_1 = (f_c + 3f_m)$, generated by the

cubic term, $c_3 s_i^3(t)$, in Equation (2.3). It follows that, for two equal-power inputs tones, an increase of x dB in the input power results in an increase of x dB in the *wanted* output signal power and an increase of 3x dB in the *third-order* IM products (IM3) as shown by the dotted line, i.e., the *IM3 response* line with slope of 3 represents

IM3 *output* power$_{[\text{in dBm}]}$ = 3.(signal *input* power)$_{[\text{in dBm}]}$ + {OIP3-3.(IIP3)}$_{[\text{in dBm}]}$

where OIP3 and IIP3 are the equivalent IM3 *output* power and signal *input* power at the *third-order intercept point* (IP3).

In other words, the power ratio of the *ouput* signal to its third-order IM product is reduced by 2x dB for an increase of x dB in the input power. This *signal-to-IM3 output* power ratio can be calculated as the difference between the *ideal* signal response and *IM3* response lines in Figure 2.6. For reference in calculation, the *third-order intercept point* is introduced as a conceptual point at which this power ratio is zero, i.e., the *output* signal power is *conceptually* equal to the power of its third-order IM product, OIP3. The *third-order intercept point* provides a figure of merit to characterize the IM distortion (IMD) performance of an amplifier. The higher the IP3, the higher the input level at which IMD becomes significant. This will result in the lower the IMD at a given signal level.

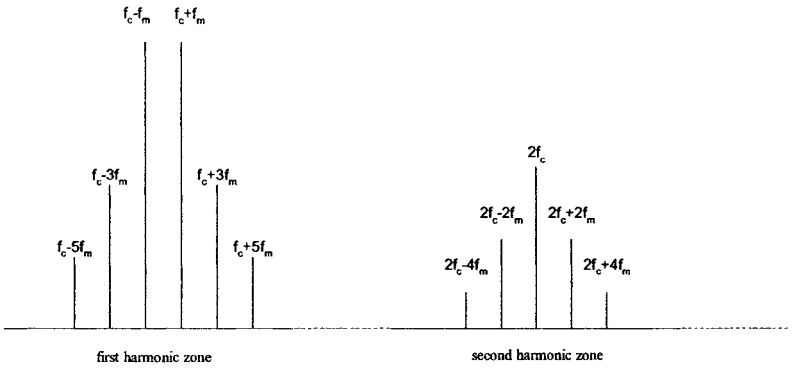

Fig. 2.7: Intermodulation products and harmonics

2.2.2 Nonlinear distortion effects on QAM signals

The amplitude to amplitude distortion distorts the symbol constellation, which make

the system more vulnerable to noise as shown in Figure 2.8. In the figure, the cross points are the un-distorted symbols. It can be seen that the symbols closer to the origin suffer less distortion than the ones further away due to their lower amplitude.

Figure 2.9 shows the power spectrum density of the output signal of a power amplifier for the case of linear (non-distortion) and AM-AM distortion. It is clear that the AM-AM distortion introduces spectral regrowth, increasing the out-of-band emission that may cause interference to adjacent channels.

Amplitude to phase distortion is the change in phase between the input and output signal of the power amplifier according to the input amplitude. The phase distortion makes the symbols on the constellation twist their angles as shown in Figure 2.10. Similar to the AM-AM distortion, the symbols further away from the origin suffer more distortion. Figure 2.11 shows the power spectrum density of the signal output for the case of linear and AM-PM distortion.

In summary, both AM-AM and AM-PM nonlinearities create distortions in the signal and spectral regrowth, and hence need some correction at the transmitter side.

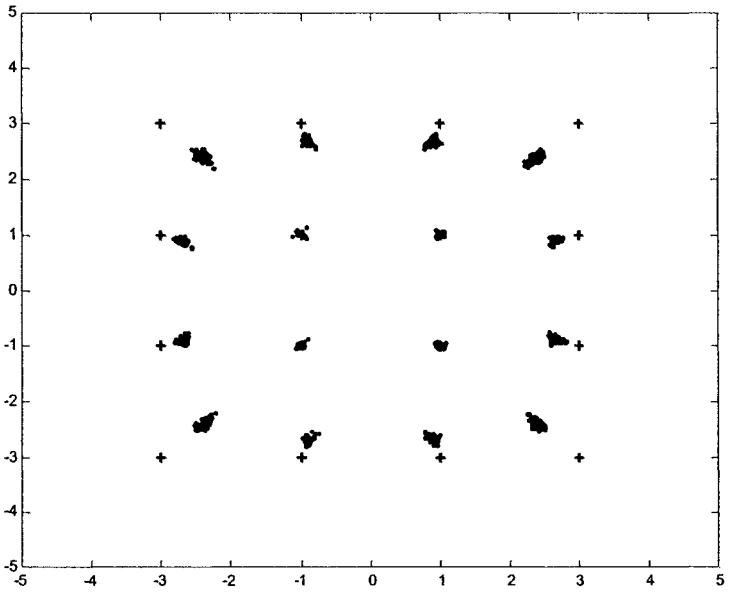

Fig. 2.8: Constellation with AM-AM distortion

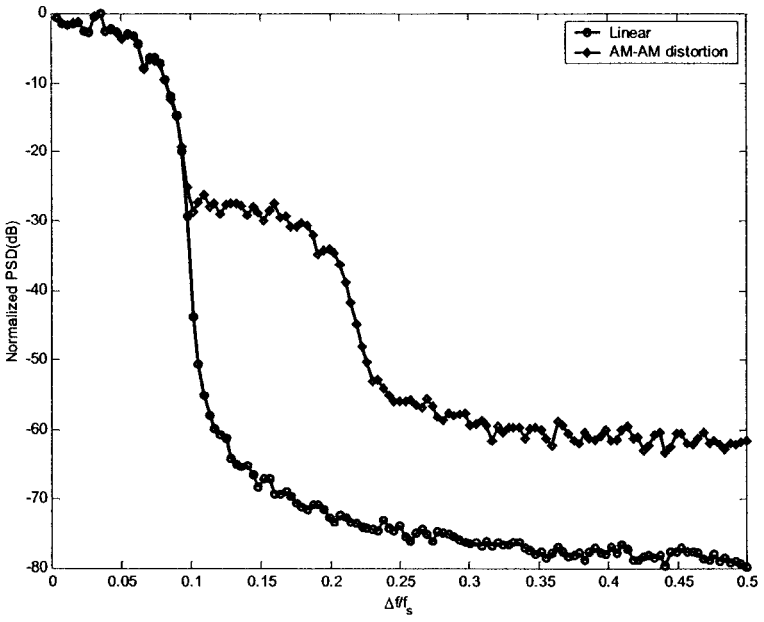

Fig. 2.9: PSD of the amplifier output with AM-AM distortion

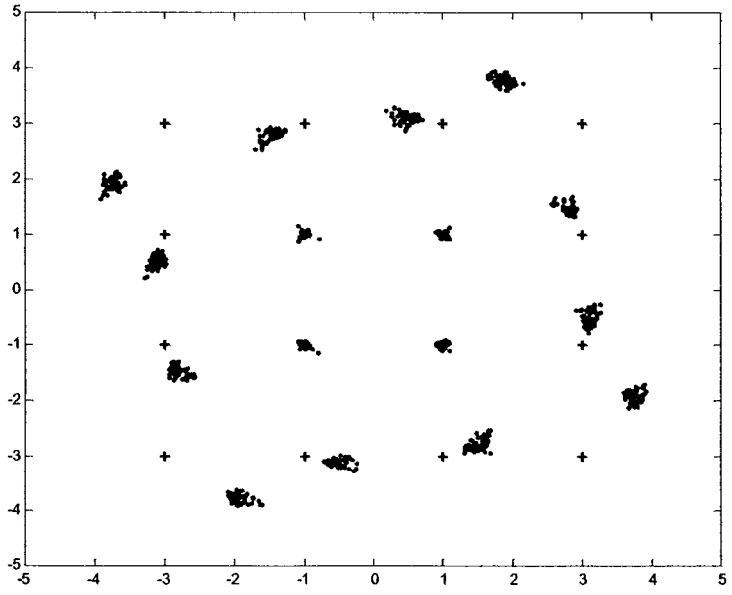

Fig. 2.10: Constellation with AM-PM distortion

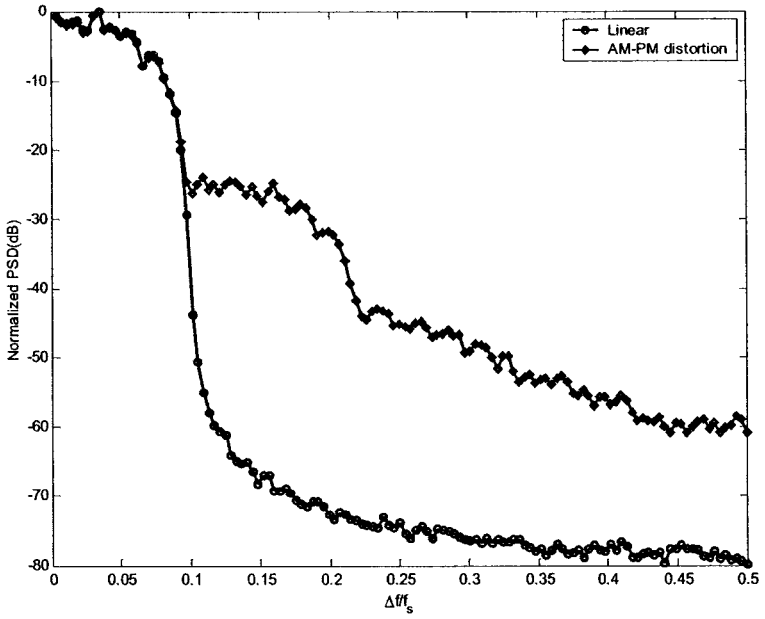

Fig. 2.11: PSD of the amplifier output with AM-PM distortion

2.3 Linearization techniques

Linearization techniques have been introduced to reduce signal distortions and out-of-band emission while operating the power amplifier near saturation to achieve its highest power efficiency. They can be categorized into two groups. The first group aims to cancel or reduce the IMD generated by the power amplifier by using feedforward or feedback techniques. The second group aims to transform the input signal to a specific format before it can be applied to the non-linear power amplifier(s) so that the IMD cannot be generated (e.g., LINC, CALLUM)

2.3.1 Feedforward linearizers

Figure 2.12 shows a transmitter using feedforward linearizer. It comprises the non-linear power amplifier an the remaining linearization circuitry including an auxiliary amplifier, four directional couplers, C_1, C_2, C_3, C_4, an attenuator A and two delay

elements T_1, T_2. The auxiliary amplifier has a power handling capacity about ten times less than the main power amplifier [2].

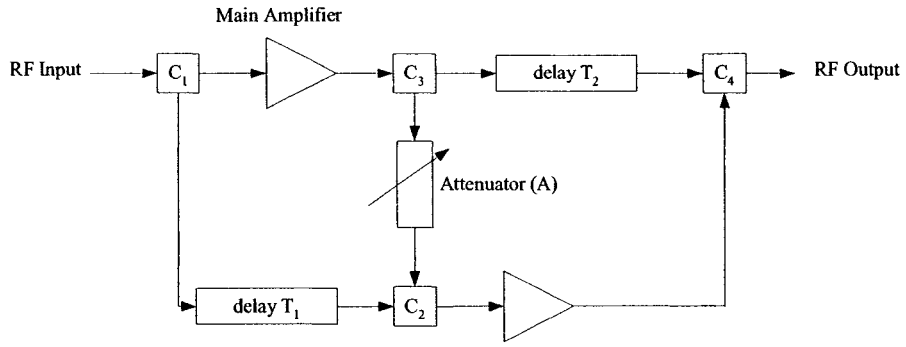

Fig. 2.12: Transmitter using Feedfoward linearizer

A signal is fed to the main power amplifier via the coupler C_1, a small sample of this signal is also fed to the delay element T_1 and then to the coupler C_2. A small sample of the distorted output from the main power amplifier is fed to the attenuator via the coupler C_3. The attenuator reduces the signal power corresponding to the power of the output signal coming to C_2 from the delay T_1. The resulting output from the coupler C_2 is the error signal. This error signal is applied to the auxiliary amplifier and removed from the distorted output of T_2 at the coupler C_4.

The disadvantage of this method is that it requires perfect gain match in the different signal path. For high frequency application, the performance of this scheme is not only dependent on the amplitude match but also on the phase/delay match along the parallel signal arms to obtain perfect signal and distortion cancellation. Many other factors such as component aging, temperature drift, etc.... cause variation that requires automatic control of amplitude gain and phase matching network [2]. Assume the main power amplifier is power efficient, the total power can still be drained due to the lost of power in the coupler, delay and the auxiliary amplifier. It implies that a high power efficient auxiliary power amplifier should be used. Moreover, it should be linear so no additional distortion is introduced to the system.

2.3.2 Feedback Linearizers

A basic negative feedback configuration is shown in Figure 2.13.

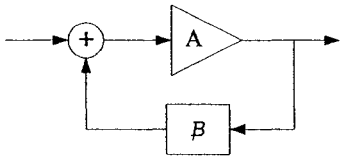

Fig. 2.13: Transmitter with negative feedback linearizer

The distortion generated by the amplifier A is reduced by an amount equal to the return different of feedback system, $F = 1 + \beta$. For larger value of loop gain, βA, the gain of this feedback system is approximately equal to $1/\beta$.

There are several feedback schemes. The most well known and widely used technique is Cartesian feedback. Figure 2.14 shows the configuration of Cartesian feedback system [3].

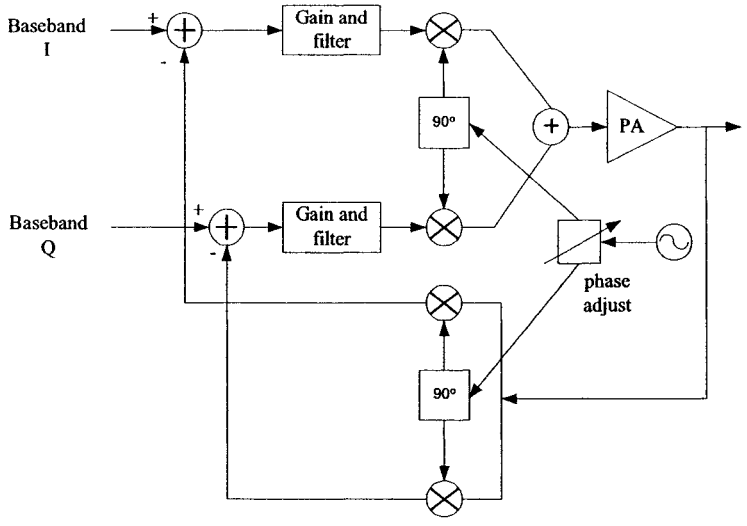

Fig. 2.14: Transmitter using Cartesian feedback linearizer

Unlike the feedforward technique, the error signal in this scheme is computed before the signal is fed to the amplifier. The output of the amplifier is synchronous demodulated and compared with the source signal to produce the error signal. The error signal is then fed to the loop filter and then modulated by the quadrature modulator block and finally it

is passed to the power amplifier. The loop control characteristics are established by the loop filter. The loop gain controls the reduction level of the intermodulation distortion, and the compensation controls the stability and behavior of the system [3]. Before the error signal is computed in baseband, the feedback needs to be demodulated. The forward and feedback are synchronized to the same carrier. However due to the RF path different, a phase adjust is to maintain a correct relationship between the input and feedback signals.

The main disadvantages of this feedback scheme is that it is only conditionally stable and the characteristic of the amplifier effectively degrade the gain phase margin of the loop.

2.3.3 LINC/CALLUM

Both LINC (linear amplification with nonlinear components) and CALLUM (combined analogue locked loop universal modulator) methods avoid the non-linear characteristic of the power amplifier by feeding it with a constant envelope signal.

Figure 2.15 shows the diagram of LINC transmitter [27]

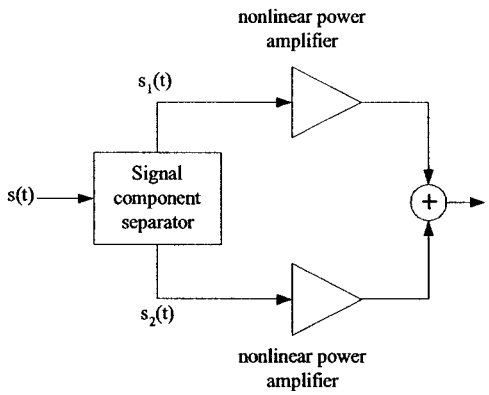

Fig. 2.15: LINC transmitter block diagram

The signal component separator splits the input signal into two constant amplitude but phase modulated signals S_1, S_2. The two phasor signals are then fed to two separated power amplifiers and finally combined to form an output signal. Since the input signal to

each amplifier has constant amplitude, no distortion is introduced to the system. The main problem with this technique is the complexity of the signal component separator and the difficulty to maintain the input signals to the power combiner to be identical in order to avoid the power losses.

Similar to LINC, CALLUM also combines two constant-amplitude phasors to form the output signal. However, instead of using signal component separator, CALLUM uses feedback to generate the two constant-amplitude signals as shown in Figure 2.16.

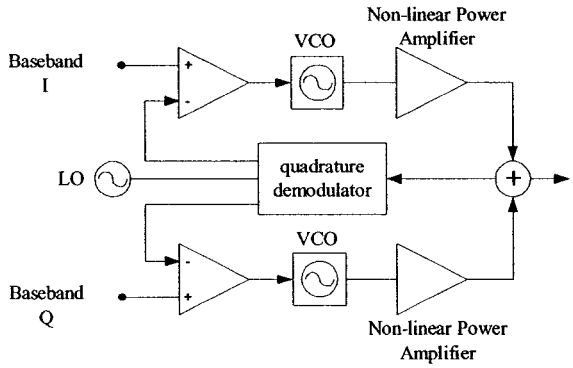

Fig. 2.16: CALLUM block diagram

The CALLUM method is susceptible to instability when the magnitude of the input signal becomes zero [28].

The disadvantage of both methods are the requirements of the two power amplifiers and the need of the power combiner.

2.4 Predistortion Techniques

The predistortion technique has been proposed as a potential solution to overcome the non-linear distortion effects [5,6]. Basically, these techniques aim to introduce "inverse non linearities that can compensate the AM/AM and AM/PM distortion generated by the nonlinear amplifier. Similar to the Cartesian feedback scheme, the correction is done to the power amplifier input. The basic principle of the predistorter is to minimize the error between the input to and the output from a non-linear power amplifier. The predistortion techniques have been divided into two categories. The first one is based on predistorting

the signal constellation in such a ways that the distortion introduced by the combination of the high power amplifier (HPA) nonlinearity and the channel memory is cancelled [8,9,10]. A realization of such technique can be made by using one the following approaches: Volterra series [11], artifical neural network [12], pth order inverse of a Volterra series [13], Hammerstein model for the predistorter [14]. The main problem of these kind of techniques is the high computational complexity and the dependence of the convergence rate and steady state performance on the size of the transmitted alphabet. The second category uses a memoryless nonlinear device placed between the shaping filter and the HPA. This type of predistorter can be implemented digitally using mapping predistorter (lookup table) technique or polynomial functions based on Cartersian or polar representation.

2.4.1 Mapping (table lookup) techniques

Mapping predistortion technique uses memory to store the output corresponding to the input. Typically, the input range of the amplifier is divided into a number of intervals which are represented by the lookup table addresses. Obviously, smaller interval corresponding to larger table size will give result higher accuracy. For every signal input, there will be a corresponding output from the table. The output value from the table combining with the input will eventually be fed to the power amplifier so that the total effect is to produce a linear response output. The first successful work using a two-dimensional lookup table technique with adaptive digital feedback at baseband was proposed by Nagata [6]. Figure 2.17 shows the block diagram of the mapping predistortion. The advantage of this technique is that it can correct any order of nonlinearity and any modulation technique. However, the size of the lookup table made the convergence time very long. Nagata [6] presented an experiment for a system with 10kHz modulation bandwidth, 128kHz sampling rate and 145MHz carrier frequency. The table size is 2M words. The convergence time was reported to be about 10 seconds. Cavers [15,16,17] has proposed to use one-dimensional lookup table using Catersian coordinates and Faulkner *et al* [18] have presented a method based on polar coordinates and one-dimensional lookup table.

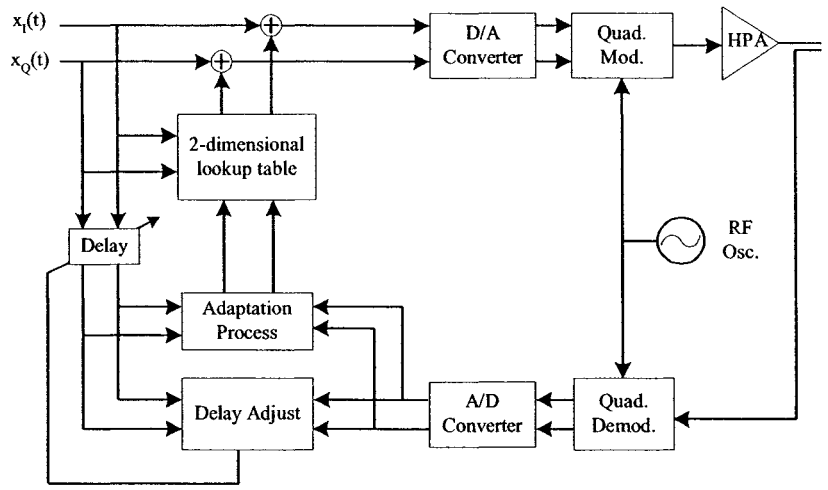

Fig. 2.17: Mapping predistorter block diagram

2.4.2 Polynomial predistortion techniques

In order to increase the rate of convergence and reduce the complexity of the mapping technique, several adaptive polynomial predistorters have been proposed. The polynomial predistorters operate with the assumption that the inverse response of the amplitude gain, phase or I and Q components of the amplifier can be modelled as finite-order polynomials. A polynomial predistorter, which operates on the amplitude gain and phase of the amplifier is classified as polar polynomial predistorter. The other approach is based on the complex (I,Q) gain. This is referred as complex gain or Cartersian polynomial predistorter. The cartesian polynomial predistorter seems to have less complexity. The approach presented in [20] estimated the predistorter polynomial coefficients by minimizing the output of band intermodulation distortion. Ghaderi *et al* [21,22] proposed a fast adaptive cartesian polynomial predistorter as shown in Figure 2.18.

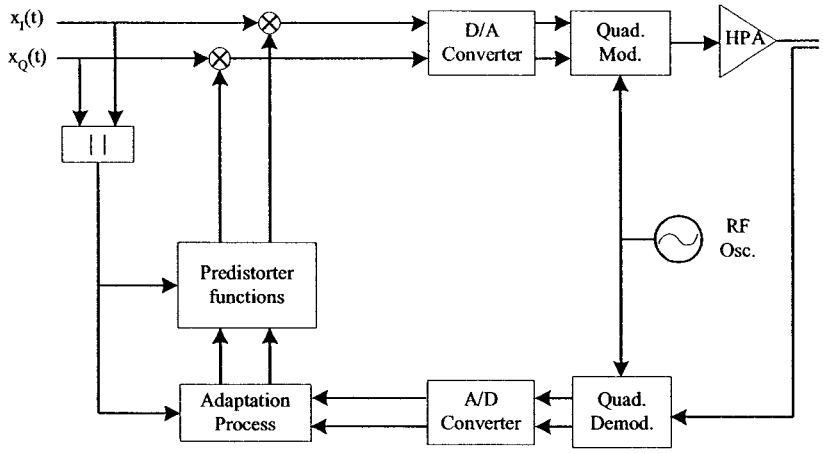

Fig. 2.18: Transmitter using polynomial predistorter

In this scheme, the authors proposed to adapt the predistortion coefficients by using a post-distorter and the RLS algorithm. The presented simulation results promised 45dB distortion suppression and about 50 iterations to converge, which is the best convergence time for predistorter reported so far in literature. The disadvantage of this technique is the high complexity comparing with other existing solutions. In [23], the polynomial polar predistorter was presented. The result obtained was claimed to have superior performance in comparison with other well-know predistortion structure with no substantial aggravation in implementation complexity. However, the adaptivity was not discussed.

Chapter 3. Polynomial Predistortion: Proposed Structure and Steady-State Performance

3.1. Structure

Figure 3.1 illustrates the block diagram of an M-QAM transmitter with the proposed predistorter.

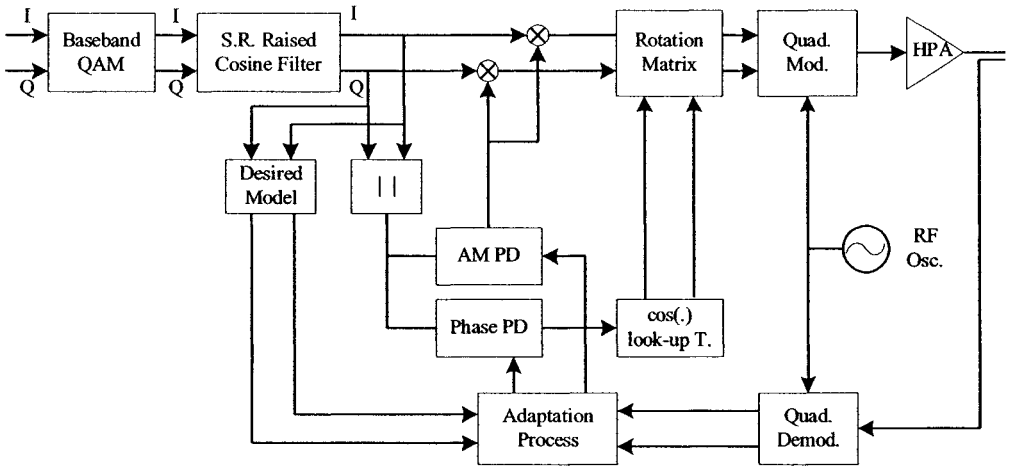

Fig. 3.1: Block diagram of the proposed predistorter

Consider a transmit power amplifier that introduces amplitude and phase distortions

depending on the input level. For an input voltage signal v_{in}

$$v_{in}(t) = r(t)\cos(\omega_c t + \theta(t)) \tag{3.1}$$

the output of the power amplifier can be written as

$$v_o(t) = G(r(t))\cos(\omega_c t + \theta(t) + \Phi(r(t))) \tag{3.2}$$

where $r(t)e^{j\theta(t)}$ is the complex envelope of the *predistorted* modulated signal (e.g., shaped M-QAM signal) and ω_c represents the carrier frequency. G(.) and $\Phi(.)$ denote the amplitude and the phase transfer functions of the power amplifier.

The predistorter aims to provide its output signal *predistorted* in an inverse and complementary manner to the distortion produced by the HPA.

Consider the filtered complex baseband signal:

$$v_m(t) = x_I(t) + jx_Q(t) = r_m(t)e^{j\theta_m(t)} \tag{3.3}$$

as the input of the predistorter. The predistorter produces the corresponding output predistorted signal $v_d(t) = r(t)e^{j\theta(t)}$ where:

$$v_d(t) = F(r_m(t))e^{j(\theta_m(t) + \Psi(r_m(t)))} \tag{3.4}$$

The functions $F(.)$ and $\Psi(.)$ are used in order to invert the nonlinearity introduced by the power amplifier, i.e.,

$$\begin{cases} G(F(r_m(t))) = \delta r_m(t) \\ \Psi(r_m(t)) + \Phi(F(r_m(t))) = 0 \end{cases} \tag{3.5}$$

where $\delta r_m(t)$ is the desired linear model.

By imposing the output power to be smaller than the amplifier saturated power, P_{sat}, Equation (3.5) involves the inversion of a bijective function G in "working domain". Since G and its inverse are continuous and C^{∞} (see Figures 3.2 and 3.3) in "working domain", the inverse function can be approximated by a polynomial expansion series of

r.

In other words, the amplitude and phase predistortion functions $F(.)$ and $\Psi(.)$ are modeled by polynomials:

$$\begin{cases} F(r) = f_1 r + f_3 r^3 + \ldots + f_{2L-1} r^{2L-1} = V^T R_f \\ \Psi(r) = \psi_0 + \psi_1 r + \psi_3 r^3 + \ldots + \psi_{2K-1} r^{2K-1} = P^T R_\psi \end{cases} \tag{3.6}$$

where $R_f = [r, r^3, \ldots, r^{2L-1}]^T$, $R_\psi = [1, r, \ldots, r^{2K-1}]^T$, $V = [f_1, f_3, \ldots, f_{2L-1}]^T$ and $P = [\psi_1, \psi_3, \ldots, \psi_{2K-1}]^T$. Note that the even coefficients in the gain and phase polynomial functions are set to zero to simplify the equations (except for the case of ψ_0), because they have no effect on the intermodulation distortion [27, 29].

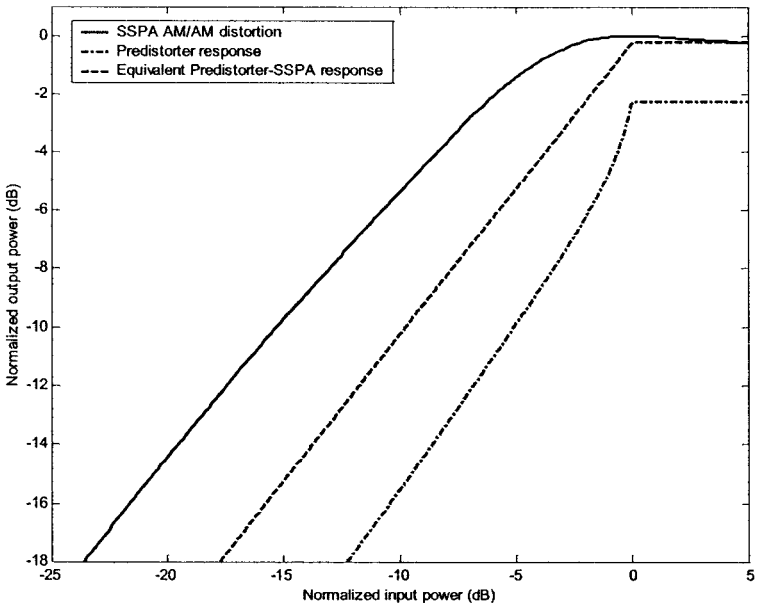

Fig. 3.2: AM/AM characteristics of the amplifier, predistorter and predistorter-amplifier

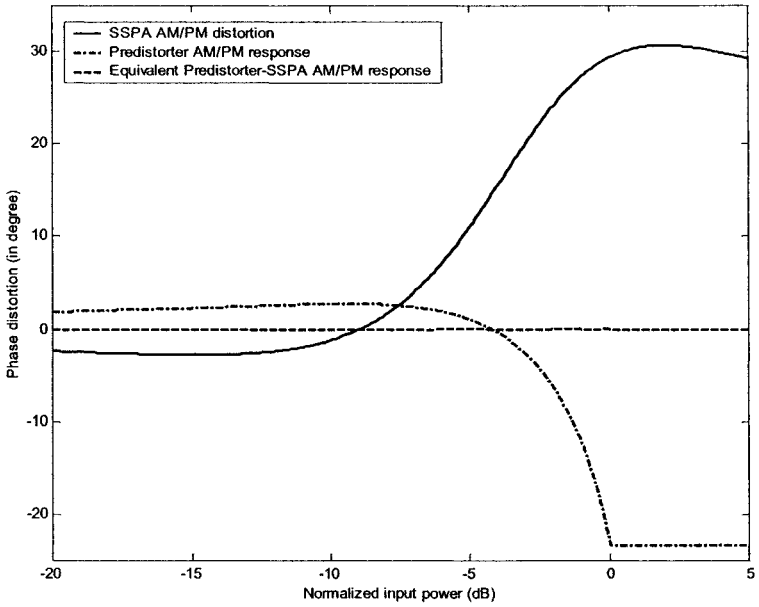

Fig. 3.3: AM/PM characteristics of the amplifier, predistorter and predistorter-amplifier

By including the term ψ_0 in the expression of $\Psi(r)$ (Eq. 3.6), we can cancel the phase shift caused by the modulator/demodulator imperfection. It is quite difficult to linearize the power amplifier up to its saturated output power P_{sat} [15]. Thus the maximum output power of the linearized power amplifier is $S \cdot P_{sat}$, where $0 < S < 1$. S represents the peak backoff (PBO) of the power amplifier [15], i.e.,

$$PBO = -10log_{10}(S) \tag{3.7}$$

We normalize the value of the input to the predistorter by imposing the input range for the linear part of predistorter/power-amplifier as:

$$0 \leq r \leq 1 \tag{3.8}$$

Now, we can evaluate δ, defined in (3.5), by:

$$\delta = \sqrt{S \cdot P_{Sat}} \tag{3.9}$$

In other words, the choice of δ will determine the minimum PBO of the proposed predistorter. The output backoff (OBO) in dB is defined by [15]:

$$OBO = 10log_{10}(P_{Sat}) - 10log_{10}(\bar{P}) \tag{3.10}$$

where $\bar{P}$ is the average power of the transmitted signal. Large OBO values will imply inefficient operation.

Next, we will evaluate the steady-state performance of this predistorter structure in terms of inter-modulation distortion and total degradation, and investigate the predistortion-order and quantization effects. Note that the coefficients of the amplitude and phase predistorter polynomial functions used in the simulations to evaluate the steady state performance are obtained by the adaptive algorithms which will be discussed in chapter 4. During these simulations, the coefficients are held fixed and the adaptation process is turned off. The characteristics of the solid state power amplifier (SSPA) model [30] used in the simulation are shown in the Figure 3.2 and 3.3.

3.2. Inter-modulation Distortion

The level of inter-modulation distortion (IMD) depends on the kind of the modulation technique [27]. In general, HPA operating near saturation introduces more IMD. There are two widely used techniques to measure the spectral purity of a transmitted signal. The simple one is the one-tone test. In this test, a tone is applied to the transmitter and the resulting IMD is measured. The second technique involves transmitting a modulated signal and measuring the out-of-band power [27].

In Figure 3.4, we plotted the spectra of transmitted signal in the case of one-tone test. The tone frequency is selected to be equal to the symbol rate, f_{symbol} ($f_{sampling} = 32f_{symbol}$). The power spectrum is normalized to have the maximum value at the $0dB$ reference. Even with a large $PBO = 10dB$, the HPA introduces an IMD of up to $-40dB$. Using the proposed predistorter with polynomial order of 7 ($L = K = 4$), the IMD can be reduced to less than $-60dB$ when the HPA operates near saturation with

a $PBO = 0.22dB$.

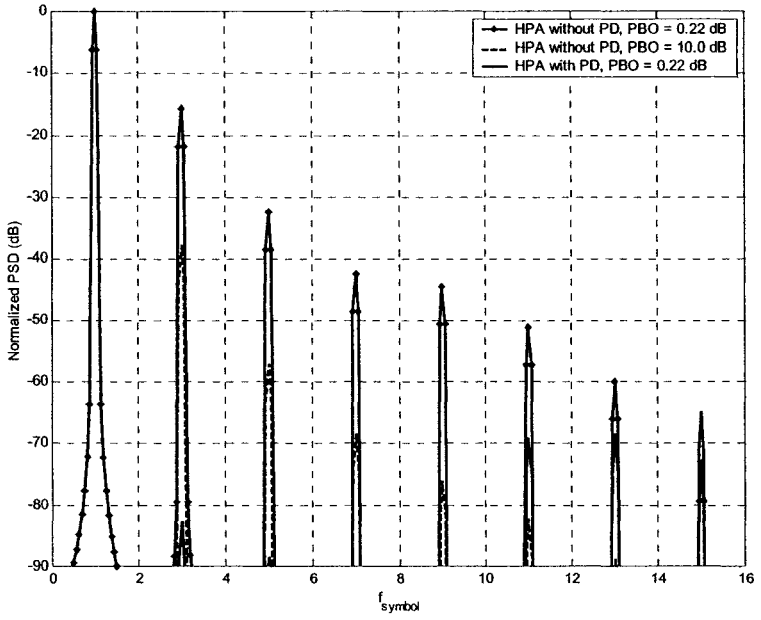

Fig. 3.4: IMD with one-tone test

Figure 3.5 shows the power spectra of the transmitted 64QAM signal in the cases with and without predistorter and for several values of PBO. The roll-off factor of the SRRC filter is 50%. The results show a significant improvement given by the proposed predistorter in terms of out-of-band power level. for PBO of $0.08dB$: at an offset frequency in the range of $1.0f_{symbol}$ to $1.5f_{symbol}$, the power spectral density with predistortion is about $40dB$ lower than that without predistortion.

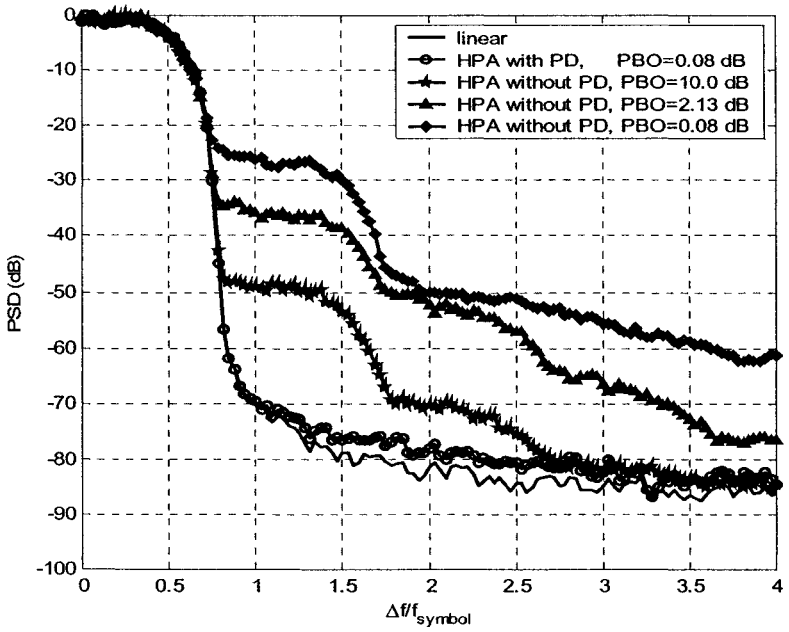

Fig. 3.5: Power Spectra of filtered 64 QAM signals with and without predistorter

The noise-free signal constellations at the receiver in the cases with and without predistortion are shown in Figures 3.6 and 3.7, respectively. Without predistortion and $PBO = 1.0dB$, the constellation is severely distorted in both amplitude and phase. This will definitely degrade the BER performance of the system. When the predistorter is introduced, even with the $PBO = 0.22dB$, Fig. 3.7 shows a significant improvement, and the constellation is very close to that in the linear region. Using simulation, we verify that the degradation in BER performance is negligible.

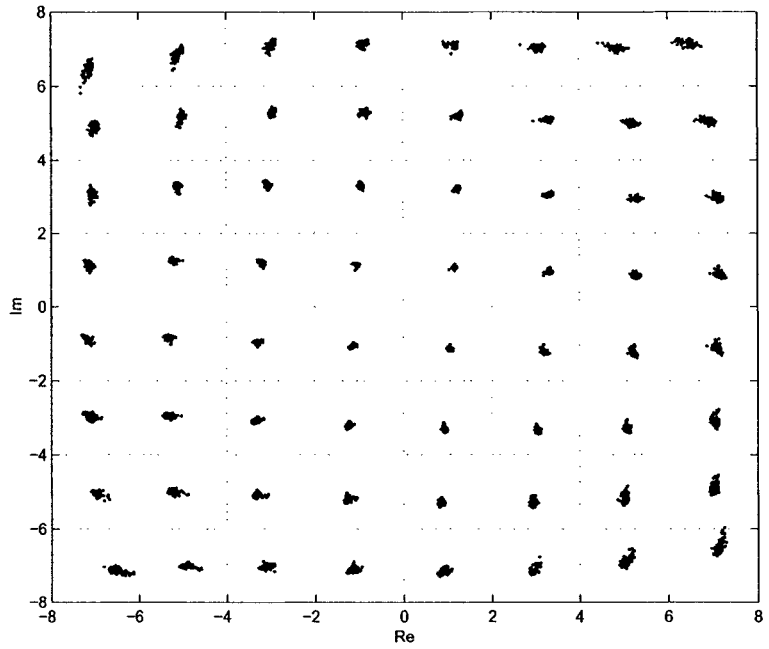

Fig. 3.6: Constellation of 64 QAM signal at the receiver output without predistorter, PBO=1dB

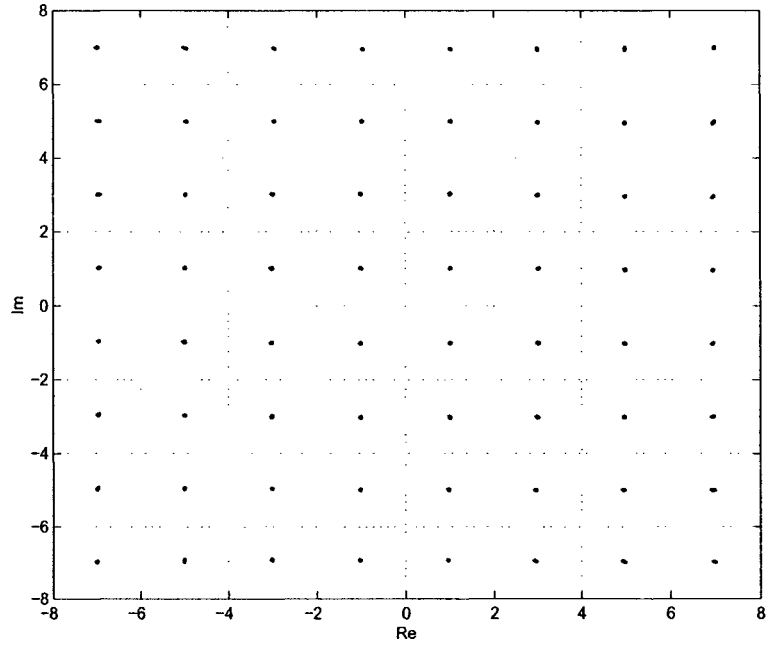

Fig. 3.7: Constellation of 64 QAM signal at the receiver output with a 7^{th}-order polynomial predistorter, PBO=0.22dB

3.3. Total Degradation

Another typical performance measure to quantify the effects of nonlinear distortion in a solid state power amplifier (SSPA) on the system performance is the total degradation (TD) in dB defined by [23]:

$$TD = OBO + \Delta_{SNR} \tag{3.11}$$

where Δ_{SNR} represents the SNR degradation due to the non-linearity of the HPA, at a given symbol error rate (e.g., $SER = 10^{-4}$). The parameter Δ_{SNR} is related to OBO. An OBO close to $0dB$ leads to an infinite value of Δ_{SNR}. On the other hand, for a very high OBO, Δ_{SNR} approaches zero and TD is close to OBO. In other words, there is an optimum value of OBO, OBO_{opt} corresponding to the minimum total degradation TD_{min}. The smaller is TD_{min}, the more efficient the predistortion technique is.

The total degradation versus OBO for 64QAM modulation is plotted in Figure 3.8. For a roll-off factor (α) of 25%, the minimum total degradation in the cases with and without predistorter are $8dB$ and $11.2dB$, respectively. One can note that the predistorter-HPA with OBO of $8dB$ can provide the same performance at $SER = 10^{-4}$ as in the ideal linear case.

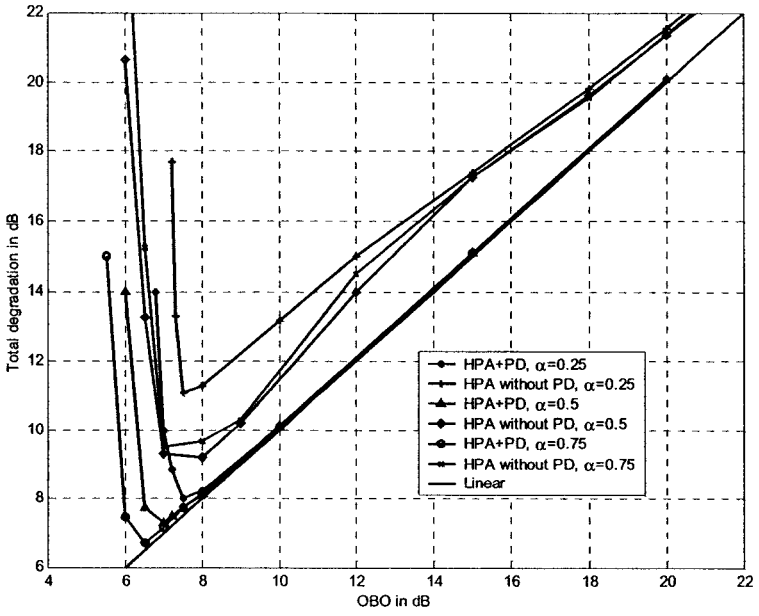

Fig. 3.8: Total degradation versus HPA OBO For SER=10^{-4}, 64QAM

3.4. Effects of Predistortion Order

The effect of the non-linearity order on the steady-state performance of the predistorter in terms of the mean-square error (MSE) is studied. We assume amplitude and phase polynomials having the same order ($L = K$). Table 3.1 shows the MSE for different polynomial orders and various filter roll-off factors. It is noted that the value of MSE may also depend on the adaptive algorithm (discussed in chapter 4) in use. The transmitted signal is 64QAM and $PBO = 0.22dB$. It is worth noting that for polynomial order greater than 7, the proposed predistorter achieves a very small MSE. When the order of polynomial is greater than 9, there is very little improvement of MSE.

Figure 3.9 shows the effects of the polynomial order on the spectral performance of 64QAM signaling scheme using a predistorter. For a low-order polynomial (smaller than 5), the out-of-band emission of the output signal is about $10dB$ worse than that of a 7^{th}-

order polynomial predistorter at an offset frequency $\Delta f = 1.3 f_{symbol}$ to $3 f_{symbol}$. However, the out-of-band emission of the 7th- and 9th-order polynomial predistorters are almost the same. In other words, an order of 7 seems to be adequate.

MSE in dB			
Polynomial order	α = 0.25	α = 0.5	α = 0.75
5	-47.40	-49.57	-47.64
7	-62.33	-63.62	-63.05
9	-66.83	-66.89	-66.41

Table 3.1: Effects of polynomial order on predistorter performance (64QAM, PBO=0.22dB)

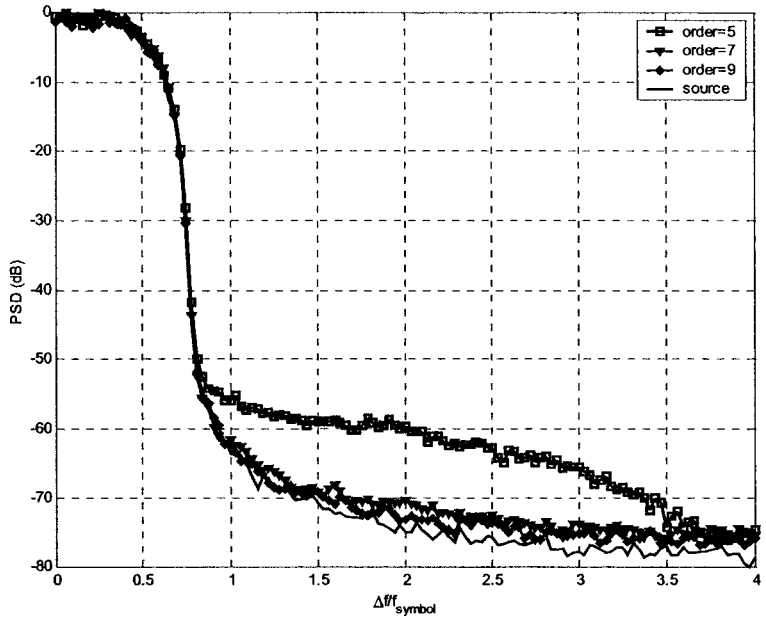

Fig. 3.9: Effect of polynomial order on spectral regrowth

3.5. Quantization Effects

Several DSP implementations of predistorter linearizer systems have been reported in literature [6],[19],[18]. With today 16 or 32 bits architectures, DSP implementation is very easy to realize and provide sufficiently accurate calculation comparing with the results obtained from the floating point simulation. A main disadvantage of DSP implementation is low execution speed and high power consumption. ASIC devices "improve these disadvantages" seen in the DSP implementation by optimizing the design at very low level hardware. One of many issues in optimizing a design for ASIC implementation is the number of bits (wordlength) to represent a number in the system. For ASIC implementation, a designer have a freedom on choosing number of bits (wordlength); while in DSP system, the wordlength is normally fixed. The choice of wordlength directly relates to the complexity of the system, and therefore the power consumption. Ideally, we want to have the wordlength as short as possible so that the complexity of the system is reduced. However, shortening the wordlength will introduce quantization noise to the system. This, in turn, will reduce system performance.

We examine the quantization effects to establish the relationship between the wordlength and the system performance in term of out-of-band emission.

As shown in Figure 3.1, on the signal path of the predistorter (excluding the adaptive processes), there are four main blocks: rotation matrix, amplitude gain predistorter, phase predistorter and cosine look-up table. The rotation matrix can be done using cordic algorithm. Quantization analysis of cordic algorithm was presented in [31]. Here, we will not discuss the implementation of the cordic algorithm, nor its quatization effect on the system performance. The rest of this section will present the analysis of the effect of coefficient quantization for the amplitude gain and phase predistorter polynomials. The effect of the look-up table size on the system performance in the polar to rectangular conversion operation will also be discussed.

3.5.1. Quantization Effects of Predistorter Phase Coefficients

Consider the phase of the signal at the output of the amplifier θ_o,

$$\theta_o(r) = \theta_i(r) + \Psi(r) + \Phi(F(r)) \tag{3.12}$$

where $\theta_i(r)$ is the phase of the input signal to the predistorter, $\Psi(r)$ is the predistorted phase, and $\Phi(F(r))$ is the amplifier distorted phase.

When the phase predistorter function converges,

$$\Psi(r) + \Phi(F(r)) \approx 0 \tag{3.13}$$

Introducing a quantization error $\Delta\psi$ in $\Psi(r)$, the phase of the signal at the output of the amplifier becomes,

$$\theta_o^q(r) = \theta_i(r) + \Psi(r) + \Delta\psi + \Phi(F(r)) \tag{3.14}$$

The phase error of the output signal due to this quantization error $\Delta\psi$ is

$$\begin{aligned} e_{\theta,\,\Delta\psi}(r) &= \theta_o^q(r) - \theta_o(r) \\ &= \Delta\psi \end{aligned} \tag{3.15}$$

At the steady state, the signal output becomes,

$$s_r^q = s^q(r) = \delta r e^{j(\theta_i + e_{\theta,\,\Delta\psi}(r))} \tag{3.16}$$

The signal output without any quantization error is,

$$s_r = s(r) = \delta r e^{j(\theta_i)} \tag{3.17}$$

Therefore, the signal output error due to the quantization $\Delta\psi$ at the time i can be written as (to make the equation more readable, we drop the r parameter in the function

expression).

$$\begin{aligned} e_{s,\Delta\psi,i} &= \delta r_i e^{j(\theta_i + e_{\theta,\Delta\psi,i})} - \delta r_i e^{j(\theta_i)} \\ &= \delta r_i e^{j\theta_i}\left(e^{je_{\theta,\Delta\psi,i}} - 1\right) \\ &= \delta r_i e^{j\theta_i}(\cos(e_{\theta,\Delta\psi,i}) + j\sin(e_{\theta,\Delta\psi,i}) - 1) \end{aligned} \tag{3.18}$$

The absolute square error of $e_{s,\Delta\psi,i}$ is expressed as,

$$\begin{aligned} \left|e_{s,\Delta\psi,i}\right|^2 &= (\delta r_i)^2((\cos(e_{\theta,\Delta\psi,i}) - 1)^2 + \sin(e_{\theta,\Delta\psi,i})^2) \\ &= (\delta r_i)^2(\cos(e_{\theta,\Delta\psi,i})^2 - 2\cos(e_{\theta,\Delta\psi,i}) + 1 + \sin(e_{\theta,\Delta\psi,i})^2) \\ &= (\delta r_i)^2(2 - 2\cos(e_{\theta,\Delta\psi,i})) \end{aligned} \tag{3.19}$$

Since $e_{\theta,\Delta\psi,i}$ is small angle; therefore,

$$\begin{aligned} \left|e_{s,\Delta\psi,i}\right|^2 &\approx 2(\delta r_i)^2\left(1 - \left(1 - \frac{e_{\theta,\Delta\psi,i}^2}{2}\right)\right) \\ &= (\delta r_i)^2 e_{\theta,\Delta\psi,i}^2 \end{aligned} \tag{3.20}$$

Assume that the quantized coefficients of the phase polynomial function are $\psi_0^q, \psi_1^q, \ldots, \psi_{2K-1}^q$. The quantized-coefficient phase predistorter polynomial function becomes,

$$\Psi^q(r) = \psi_0^q + \psi_1^q r + \psi_3^q r^3 + \ldots + \psi_{2K-1}^q r^{2K-1} \tag{3.21}$$

In order to compute the out-of-band power spectral density or out-of-band emission (OBE), we need to calculate the SNR at the output of the power amplifier [32]. The phase error of the output signal due to the quantization of the phase predistorter coefficients at

the time t_i is

$$\begin{aligned} e_{\theta,\Delta\psi,i} &= e_{\theta,\Delta\psi}(r_i) = \Psi^q(r_i) - \Psi(r_i) \\ &= \begin{pmatrix} (\psi_0^q + \psi_1^q r_i + \psi_3^q r_i^3 + \ldots + \psi_{2K-1}^q r_i^{2K-1}) \\ -(\psi_0 + \psi_1 r_i + \psi_3 r_i^3 + \ldots + \psi_{2K-1} r_i^{2K-1}) \end{pmatrix} \\ &= e_{\psi_0} + e_{\psi_1} r_i + e_{\psi_3} r_i^3 + \ldots + e_{\psi_{2K-1}} r_i^{2K-1} \end{aligned} \tag{3.22}$$

where the $\Psi^q(r_i)$ represents the phase predistortion polynomial with quantized coefficients. Assume that $e_{\psi_0}, e_{\psi_1}, e_{\psi_3}, \ldots, e_{\psi_{2K-1}}$ are independent random variables and uniformly distributed from $-\Delta/2$ to $\Delta/2$ [33].

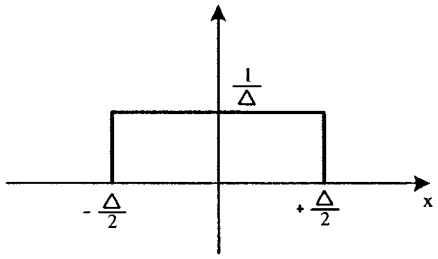

Fig. 3.10: Uniform distribution of quantization error

where $\Delta = \dfrac{2X_m}{2^B}$, X_m is the absolute maximum value of $\{\psi_0, \psi_1, \psi_3, \ldots, \psi_{2K-1}\}$ and B is the number of bits used in the quantizer.

The average error power of the amplifier output is,

$$\begin{aligned} \sigma^2_{e_{s,\Delta\psi,i}} &= E\left\{ \left| e_{s,\Delta\psi,i} \right|^2 \right\} \\ &= (\delta r_i)^2 E\left\{ \left(e_{\psi_0} + e_{\psi_1} r_i + e_{\psi_3} r_i^3 + \ldots + e_{\psi_{2K-1}} r_i^{2K-1} \right)^2 \right\} \end{aligned} \tag{3.23}$$

Because

$$E[e_{\psi_n}] = 0 \tag{3.24}$$

and

$$E[e_{\psi_n} e_{\psi_j}] = 0 \quad if\ n \neq j\ , \tag{3.25}$$

Therefore, the average error variance of the amplifier output at the time i is

$$\begin{aligned} \sigma^2_{e_{s,\Delta\psi,i}} &= \sigma^2_{e_{s,\Delta\psi}}(r_i) \\ &= E\left[e^2_{\psi_0}\right] + r_i^2 E\left[e^2_{\psi_1}\right] + r_i^6 E\left[e^2_{\psi_3}\right] + \ldots + r_i^{2(2K-1)} E\left[e^2_{\psi_{2K-1}}\right] \\ &= \frac{\Delta^2}{12}(\delta r_i)^2 (1 + r_i^2 + r_i^6 + \ldots + r_i^{2(2K-1)}) \end{aligned} \tag{3.26}$$

Taking the modulation scheme into account, the total average power in the amplifier output becomes,

$$\begin{aligned} \sigma^2_{e_{s,\Delta\psi}} &= \int_0^1 p_r(r_i)\sigma^2_{e_{s,\Delta\psi}}(r_i)dr_i \\ &= \frac{\Delta^2\delta^2}{12}\int_0^1 p_r(r_i) r_i^2 (1 + r_i^{\,2} + r_i^{\,6} + \ldots + r_i^{\,2(2K-1)})dr_i \end{aligned} \tag{3.27}$$

where $p_r(r)$ is the probability density function of the amplitude of the filtered signal input to the predistorter. The signal to noise ratio is

$$SNR_{\Delta\psi} = \frac{\sigma_s^2}{\sigma^2_{e_{s,\Delta\psi}}} = \frac{\int_0^1 p_r(r_i) r_i^{\,2} dr}{\frac{\Delta^2\delta^2}{12}\int_0^1 p_r(r_i) r_i^2 (1 + r_i^2 + r_i^6 + \ldots + r_i^{2(2K-1)})dr} \tag{3.28}$$

where σ_s^2 is the signal power. Eq. (3.28) indicates a small effect of K on SNR. The out-of-band emission (OBE) level as compared to the power spectral density at the center frequency due to the quantized coefficient error of the phase predistorter polynomial

function is [32]

$$OBE_{\Delta\psi} = \frac{f_{symbol}}{f_{sampling} \cdot SNR_{\Delta\psi}} \tag{3.29}$$

where $f_{sampling} = 8f_{symbol}$ is the sampling frequency in use.

To evaluate the SNR expressed in equation (3.28), we need to know the probability density function of the filtered signal $p_r(r)$. Figure 3.11 shows the function $p_r(r)$ for the case of the 64 QAM signal, the filter is RRCS (root raised cosine filter) with $f_{sampling}/f_{symbol} = 8$, and roll-off factor $(\alpha) = 0.5$.

Table 3.2 summarizes both analytical and simulation results on the out-of-band emission for $K = 4$ (i.e., 7^{th} order) and different wordlengths. The analytical results are obtained from Eqs. (3.28) and (3.29). In simulation, the out-of-band power and total power are directly computed from the simulated signal for different wordlengths in order to establish the SNR. The analytical and simulation results are in a good agreement with a difference in out-of-band emission of less than $0.1dB$. This confirms the accuracy of the derived equations that describe the relationship between the wordlength and out-of-band emission in Equations (3.28) and (3.29). Figure 3.12 shows the power spectra of the 64QAM signal for different wordlengths of the phase predistorter polynomial coefficients. In the figure, the spectrum of the source signal (the output of the root raised cosine filter) is plotted as the solid line. The results shown in Table 3.2 agree with the results obtained in Figure 3.12. For a required out-of-band emission of $-60dB$ at the output of the amplifier, we need at least 7 bits to represent the coefficients of the phase predistorter polynomial.

Word length	6 bits	7 bits	8 bits	9 bits
OBE (calculated)	-56.4dB	-62.4	-68.5	-74.5
OBE (simulated)	-56.5dB	-62.5	-68.5	-74.6

Table 3.2: Out-of-band emission with different quantized polynomial coefficients (phase predistorter)

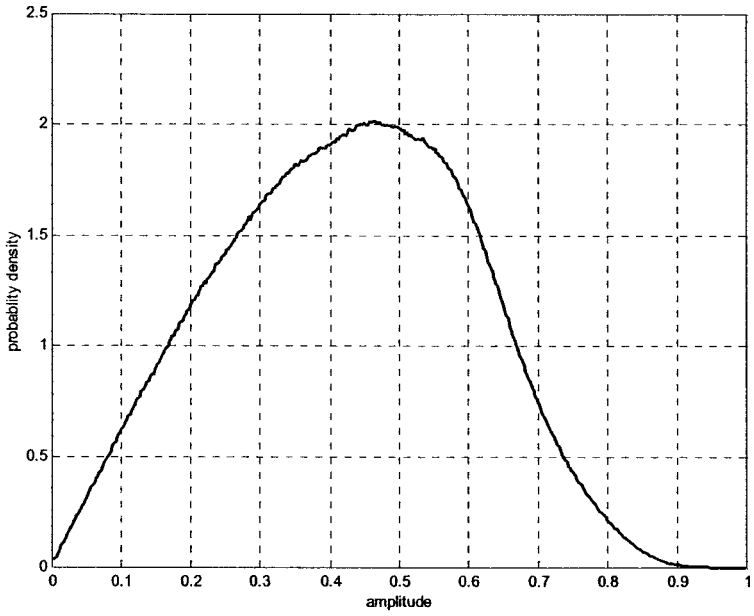

Fig. 3.11: Amplitude histogram for 64 QAM signal, SRRC with roll-off factor 0.5 (amplitude is normalized to 1)

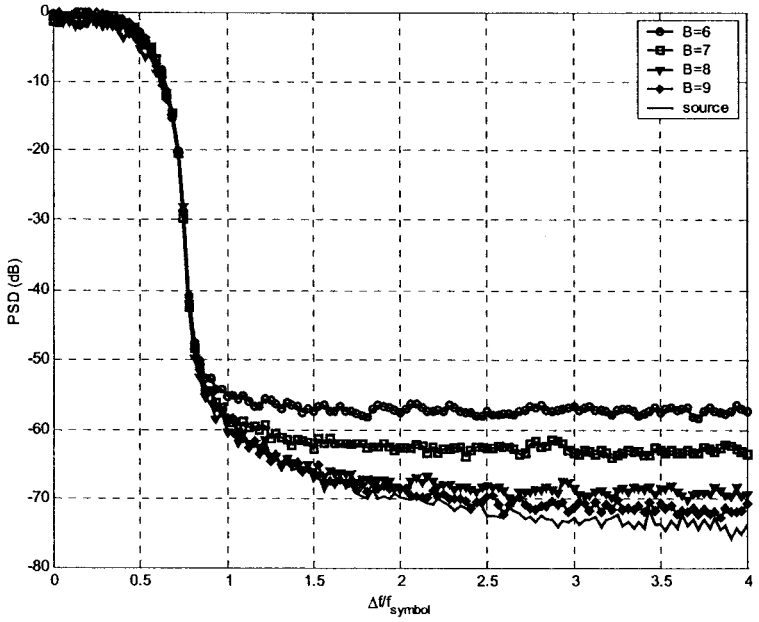

Fig. 3.12: Power spectra of 64 QAM signals for different wordlengths of the phase predistorter polynomial coefficients

3.5.2. Quantization Effects of Amplitude Gain Polynomial Coefficients

Let $\Delta r_{p,i}$ be the quantization noise, due to the quantization of the coefficients of the amplitude gain function where $r_{p,i}$ is the amplitude without noise at the output of the amplitude gain polynomial function. r_i is the amplitude of the input signal. The output signal of the amplifier can be written as,

$$s(r_{p,i} + \Delta r_{p,i}) = G(r_{p,i} + \Delta r_{p,i}) e^{j(\theta_i + \Phi(r_{p,i} + \Delta r_{p,i}) + \Psi(r_i))} \tag{3.30}$$

$G(.)$ is the amplitude gain of the power amplifier, θ_i is the phase of the input signal. $\Phi(.)$ is the distorted phase produced by the power amplifier and $\Psi(.)$ is the predistorted

phase.

Expanding the right-hand side of Equation (3.30) using Taylor's series, we obtain,

$$s(r_{p,i} + \Delta r_{p,i}) = s(r_{p,i}) + \Delta r_{p,i} s'(r_{p,i}) + \frac{1}{2!}(\Delta r_{p,i})^2 s''(r_{p,i}) + \ldots \tag{3.31}$$

Introducing the quantization error $\Delta r_{p,i}$ creates an error $e_{s,\Delta f,i}$ in the signal output of the amplifier,

$$e_{s,\Delta f,i} = e_{s,\Delta r_i} = \Delta r_{p,i} s'(r_{p,i}) + \frac{1}{2!}(\Delta r_{p,i})^2 s''(r_{p,i}) + \ldots \tag{3.32}$$

where,

$$\begin{aligned} s'(r_{p,i}) &= \frac{\partial}{\partial r_i}\left(G(r_{p,i}) e^{j(\theta_i + \Phi(r_{p,i}) + \Psi(r_i))}\right) \\ &= (G'(r_{p,i}) + G(r_{p,i})\Phi'(r_{p,i})) e^{j(\theta_i + \Phi(r_{p,i}) + \Psi(r_i))} \end{aligned} \tag{3.33}$$

and

$$\begin{aligned} s''(r_{p,i}) &= \frac{\partial}{\partial r_{p,i}}(s'(r_{p,i})) \\ &= (G''(r_{p,i}) + 2G'(r_{p,i})\Phi'(r_{p,i}) + G(r_{p,i})\Phi''(r_{p,i}) + G(r_{p,i})(\Phi'(r_{p,i}))^2) \\ &\quad e^{j(\theta_i + \Phi(r_{p,i}) + \Psi(r_i))} \end{aligned} \tag{3.34}$$

where

$$G'(r_{p,i}) = \frac{\partial}{\partial r_{p,i}} G(r_{p,i}),\ \Phi'(r_{p,i}) = \frac{\partial}{\partial r_{p,i}} \Phi(r_{p,i}) \tag{3.35}$$

and

$$G''(r_{p,i}) = \frac{\partial}{\partial r_{p,i}} G'(r_{p,i}),\ \Phi''(r_{p,i}) = \frac{\partial}{\partial r_{p,i}} \Phi'(r_{p,i}) \tag{3.36}$$

Consider only the first order terms of Taylor's series expansion,

$$e^{1}_{s,\Delta f,i} = \Delta r_{p,i}(G'(r_{p,i}) + G(r_{p,i})\Phi'(r_{p,i}))e^{j(\theta_i + \Phi(r_{p,i}) + \Psi(r_i))} \tag{3.37}$$

The absolute square error becomes,

$$\left|e^{1}_{s,\Delta f,i}\right|^2 = (\Delta r_{p,i})^2(G'(r_{p,i}) + G(r_{p,i})\Phi'(r_{p,i}))^2 \tag{3.38}$$

Let $f^q_1, f^q_3, \ldots, f^q_{2L-1}$ be the quantized coefficients of the amplitude gain polynomial function. $\Delta r_{p,i}$ can be expressed as,

$$\begin{aligned}\Delta r_{p,i} &= (f^q_1 r_i + f^q_3 r_i^3 + \ldots f^q_{2L-1} r_i^{2L-1}) - (f_1 r_i + f_3 r_i^3 + \ldots f_{2L-1} r_i^{2L-1}) \\ &= e_{f_1} r_i + e_{f_3} r_i^3 + \ldots + e_{f_{2L-1}} r_i^{2L-1}\end{aligned} \tag{3.39}$$

where $e_{f_k} = f^q_k - f_k$.

Assume that $e_{f_0}, e_{f_1}, e_{f_3}, \ldots, e_{f_{2L-1}}$ are independent random variables and uniformly distributed from $-\Delta/2$ to $\Delta/2$ [33] as shown in figure 3.10. The average noise power in the output signal of the amplifier is,

$$\begin{aligned}\sigma^2_{e_{s,\Delta f,i}} &= E\left\{\left|e^{1}_{s,\Delta f,i}\right|^2\right\} \\ &= (G'(r_{p,i}) + G(r_{p,i})\Phi'(r_{p,i}))^2\left(E\left\{\left(e_{f_1} r_i + e_{f_3} r_i^3 \ldots + e_{f_{2L-1}} r_i^{2L-1}\right)^2\right\}\right)\end{aligned} \tag{3.40}$$

Since

$$E[e_{f_n}] = 0 \tag{3.41}$$

and

$$E[e_{f_n} e_{f_j}] = 0 \quad if\ n \neq j\ , \tag{3.42}$$

Therefore, the average error variance of the amplifier output at the time i is

$$\begin{aligned}\sigma^2_{e_{s,\Delta f,i}} &= \sigma^2_{e_{s,\Delta f}}(r_i) \\ &= (G'(r_{p,i}) + G(r_{p,i})\Phi'(r_{p,i}))^2\left(r_i^2 E\left[e_{f_1}^2\right] + r_i^6 E\left[e_{f_3}^2\right] + \ldots + r_i^{2(2L-1)} E\left[e_{f_{2L-1}}^2\right]\right) \\ &= \frac{\Delta^2}{12}(r_i^2 + r_i^6 + \ldots + r_i^{2(2L-1)})(G'(F(r_i)) + G(F(r_i))\Phi'(F(r_i)))^2\end{aligned} \tag{3.43}$$

Taking into account the modulation,

$$\begin{aligned}\sigma^2_{e_{s,\Delta f}} &= \int_0^1 p_r(r_i)\sigma^2_{e_{s,\Delta f,i}}\,dr_i \\ &= \frac{\Delta^2}{12}\int_0^1 (p_r(r_i)(r_i^2 + r_i^6 + \ldots + r_i^{2(2L-1)})(G'(F(r_i)) + G(F(r_i))\Phi'(F(r_i)))^2)dr_i\end{aligned} \tag{3.44}$$

where $p_r(r)$ is the probability density function of the amplitude of the filtered signal input to the predistorter.

The SNR and out-of-band emission are,

$$\begin{aligned}SNR_{\Delta f} &= \frac{\sigma_s^2}{\sigma^2_{e_{s,\Delta f}}} \\ &= \frac{\int_0^1 p_r(r_i)r_i^2\,dr_i}{\frac{\Delta^2}{12}\int_0^1 (p_r(r_i)(r_i^2 + r_i^6 + \ldots + r_i^{2(2L-1)})(G'(F(r_i)) + G(F(r_i))\Phi'(F(r_i)))^2)dr_i}\end{aligned} \tag{3.45}$$

$$OBE_{\Delta f} = \frac{f_{symbol}}{f_{sampling} \cdot SNR_{\Delta f}} \tag{3.46}$$

Equations (3.45) and (3.46) are evaluated for different values of the wordlengths and $L = 4$. The results are shown in the second row (calculated) of Table 3.3. Note that the value of L (> 3) has a very little effect on the SNR as indicated by Eq. (3.45). The last row of the Table 3.3 shows the results obtained from simulation. The differences between the calculated and simulated values are about $1dB$ due to the first-order approximation of the Taylor's series in Equation (3.37). More accurate results can be obtained with higher-

order approximation at the cost of more complicated derivations. Figures 3.13 shows the spectra of the 64QAM signal for different wordlengths of amplitude gain predistorter polynomial coefficients. The results indicates that to have the out-of-band emission below $-60dB$, we need at least 8 bits to represent the amplitude gain.

Word length	7 bits	8 bits	9 bits	10 bits
OBE (calculated)	-55.2dB	-61.2	-67.3	-73.3
OBE (simulated)	-56.0dB	-62.1	-68.1	-74.2

Table 3.3: Out-of-band emission with quantized polynomial coefficients (amplitude gain predistorter)

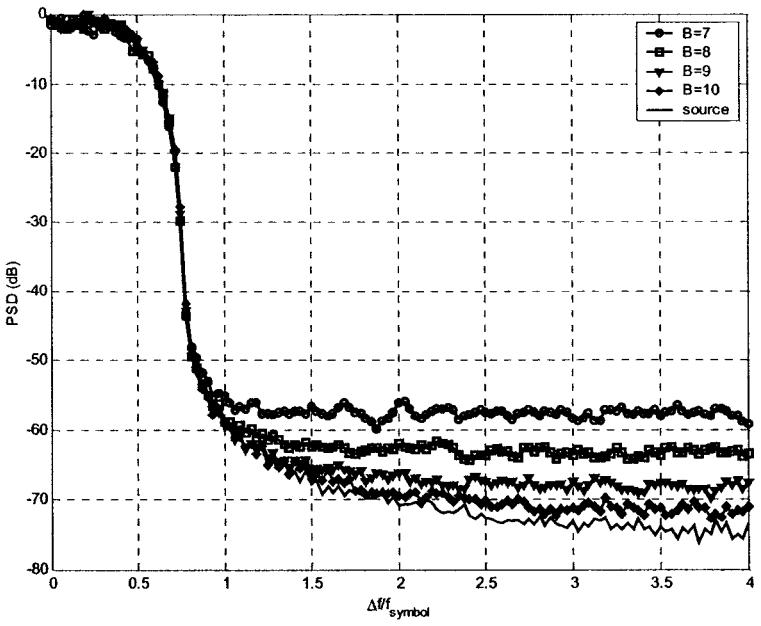

Fig. 3.13: Power spectra of 64 QAM signal for different wordlengths of the amplitude gain predistorter polynomial coefficients

3.5.3. Quantization Effects of Cos, Sine Look-up Tables

The output of the amplifier can be written as

$$s(r_i) = G(F(r_i))e^{j(\theta_i + \Psi(r_i) + \Phi(F(r_i)))} = G(F(r_i))e^{j\gamma_i} \tag{3.47}$$

where $\gamma_i = \theta_i + \Psi(r_i) + \Phi(F(r_i))$, and r_i, θ_i are the amplitude and phase of the input signal respectively. $\Psi(r_i)$ is the predistorted phase output and $\Phi(F(r_i))$ is the amplifier phase distortion.

Let $\Psi_q(r_i)$ be the predistorted phase with the consideration of quantized look-up table. The signal output of the amplifier becomes

$$s^q(r_i) = G(F(r_i))e^{j(\theta_i + \Psi_q(r_i) + \Phi(F(r_i)))} = G(F(r_i))e^{j\gamma_{q,i}} \tag{3.48}$$

where $\gamma_{q,i} = \theta_i + \Psi_q(r_i) + \Phi(F(r_i))$. Note that the phase $\Psi(r_i)$ does not affect the distortion level introduced by the power amplifier. The error of the output signal due to the quantized lookup table is,

$$\begin{aligned} e_{s,\Delta T,i} &= s^q(r_i) - s(r_i) \\ &= G(F(r_i))\left(e^{j\gamma_{q,i}} - e^{j\gamma_i}\right) \\ &= G(F(r_i))e^{j\gamma_i}\left(e^{j(\gamma_{q,i}-\gamma_i)} - 1\right) \end{aligned} \tag{3.49}$$

Because $\gamma_{q,i} \approx \gamma_i$, therefore

$$e_{s,\Delta T,i} = G(F(r_i))e^{j\gamma_i}j(\gamma_{q,i}-\gamma_i) \tag{3.50}$$

The absolute square error is,

$$\left|e_{s,\Delta T,i}\right|^2 = G^2(F(r_i))(\gamma_{q,i}-\gamma_i)^2 \tag{3.51}$$

We define $e_{\psi,\Delta T,i} = \gamma_{q,i} - \gamma_i$ as the predistorted phase error due to the quantized

lookup table.

$$\begin{aligned} e_{\psi,\Delta T,i} &= (\theta_i + \Psi^q(r_i) + \Phi(F(r_i))) - (\theta_i + \Psi(r_i) + \Phi(F(r_i))) \\ &= \Psi^q(r_i) - \Psi(r_i) \end{aligned} \tag{3.52}$$

Assume that $e_{\psi,\Delta T,i}$ is a random variable having uniform distribution [33] as shown in figure 3.10. The average noise power can be calculated as,

$$\begin{aligned} \sigma^2_{e_{s,\Delta T,i}} &= \frac{1}{\Delta}\int_{-\frac{\Delta}{2}}^{\frac{\Delta}{2}} \left|e_{s,\Delta T,i}\right|^2 de_{\psi,\Delta T,i} \\ &= \frac{1}{\Delta}\int_{-\frac{\Delta}{2}}^{\frac{\Delta}{2}} G^2(F(r_i))e^2_{\psi,\Delta T,i} de_{\psi,\Delta T,i} \\ &= \frac{\Delta^2}{12}G^2(F(r_i)) \end{aligned} \tag{3.53}$$

When the amplitude gain and phase predistorter algorithm converge, $G(F(r_i)) = \delta r_i$. Taking the modulation scheme into account, the total noise average power becomes

$$\sigma^2_{s,\Delta T} = \frac{\delta^2\Delta^2}{12}\int_0^1 p_r(r_i)r_i^2 dr \tag{3.54}$$

where $p_r(r)$ is the probability density function of the input signal amplitude of the predistorter.

The SNR and out-of-band emission are,

$$SNR_{\Delta T} = \frac{\sigma_s^2}{\sigma_{e_{s,\Delta T}}^2} = \frac{\int_0^1 p_r(r) r^2 dr}{\frac{\delta^2 \Delta^2}{12} \int_0^1 p_r(r) r^2 dr} = \frac{12}{\delta^2 \Delta^2} \tag{3.55}$$

$$OBE_{\Delta T} = \frac{f_{symbol}}{f_{sampling} \cdot SNR_{\Delta T}} \tag{3.56}$$

The simulation and analytical results on the out-of-band emission level for different numbers of bits to represent the address of an entry of the sine and cosine look-up table are shown in Table 3.4. An m-bit address corresponds to a table size of 2^m. The spectra of the 64 QAM signal for different look-up table sizes are plotted in Figure 3.14. It shows that a table of size $64=2^6$ is sufficient to obtain an out-of-band emission below -60dB at the amplifier output.

Word length	5 bits	6 bits	7 bits	8 bits
OBE (calculated)	-55.9dB	-62.0	68.0	74.0
OBE (simulated)	-56.6dB	62.7	68.1	73.9

Table 3.4: Out-of-band emission with quantized sine & cosine lookup tables

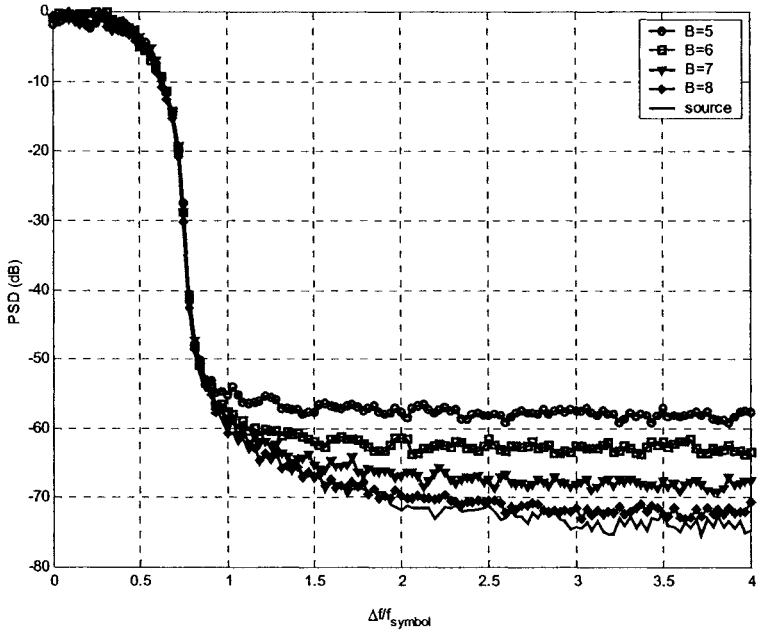

Fig. 3.14: Power spectra of 64 QAM signal for different wordlengths of the cosine look-up table

Chapter 4. Adaptive Algorithms for Polynomial Predistorters

Adaptive predistorters presented in the literature, are based on complex representation of the distortion introduced by the power amplifier. In [21,22], the authors proposed to use the RLS algorithm to compute the gains that they have to apply to the in-phase and quadrature components, in order to linearize the power amplifier. While the presented simulation results were encouraging, the adaptation approach requires a high computational complexity. In this section, we propose two adaptive algorithms for the proposed polynomial predistortion scheme. The first one is based on the least mean square (LMS) concept for its simplicity. Its slow convergence rate can be improved with a small increase in complexity. The second one is based on the recursive least square (RLS) concept for its a very fast convergence rate with a complexity lower than that in [22].

4.1. LMS-based Algorithm

The optimum coefficient vectors V and P of the predistorter are determined in order to minimize the two mean square error (MSE) functions defined by:

$$\begin{aligned} J_1(V) &= E\left((\delta r - G(V^T R_f))^2\right) \\ J_2(P) &= E\left((\Phi(V_{opt}^T R_f) + P^T R_\psi)^2\right) \end{aligned} \tag{4.1}$$

where V_{opt} is the optimal coefficient vector of the amplitude predistorter polynomial.

The least mean square (LMS) iterative algorithm related to $J_1(V))$ can be derived as follows:

$$V_{k+1} = V_k - \mu_v \nabla_V J_1(V_k) = V_k + \mu_v R_{f,k} G'(V_k^T R_{f,k})(\delta r_k - G(V_k^T R_{f,k})) \qquad (4.2)$$

where μ_v is a positive step size and G' denotes the derivative function of G

Since, $G(r)$ is a crescent function in the working area, the scalar $G'(V_k^T R_{f,k})$ is positive and one can simplify the recursive relation (4.2) to:

$$V_{k+1} = V_k + \mu_v R_{f,k}(\delta r_k - G(V_k^T R_{f,k})) \qquad (4.3)$$

where μ_v is a constant positive step size, selected to be sufficiently small to guarantee the stability of the algorithm.

The phase predistorter aims to identify the opposite of the phase shift $\Phi(F(r))$. It is much simpler than the amplitude predistortion problem. The Taylor's series expansion in r of the phase shift can be expressed by:

$$\begin{aligned} \Phi(F(r)) &= \Phi(V_k^T R_f) \\ &= -(p_{0,k} + p_{1,k} r + \ldots + p_{2L-1,k} r^{2L-1}) + O(r^{2L+1}) \\ &= -P_{opt,k}^T R_\psi + n \end{aligned} \qquad (4.4)$$

where n represents the truncation noise.

The vector $P_{opt,k}$ is time-varying, and depends on the convergence of the amplitude predistorter V_k. When the amplitude predistorter reaches the steady state, $P_{opt,k}$ becomes a constant P_{opt}

To cancel the phase shift, we have to identify P_k. This can be done using the

conventional LMS algorithm:

$$\begin{aligned} e_{\psi,k} &= -\Phi(F(r_k)) - P_k^T R_{\psi,k} \\ P_{k+1} &= P_k + \mu_\psi e_{\psi,k} R_{\psi,k} \end{aligned} \tag{4.5}$$

where μ_ψ is a positive step size.

In the next section, we will present the convergence analysis and discuss the convergence rate of the proposed algorithm.

4.1.1. Convergence Analysis

In this section, we will focus first on the analysis of the amplitude predistortion. Exact analysis of the algorithm given by (4.3) is complicated. To make the analysis tractable, we introduce the following simplifying assumptions.

Assumption 1: *The gain distortion* $G(r)$ *can be expanded using Taylor series*:

$$G(r) = g_1 + g_3 r^3 + g_5 r^5 + \ldots + g_{2N-1} r^{2N-1} + O(r^{2N+1}) \tag{4.6}$$

There exists V_{opt}, such that $G(V_{opt}^T R_{f,k}) = \delta r_k + t_k$, where t_k represents the truncation noise. From the assumption 1, Equation (4.3) can be rewritten as:

$$\begin{aligned} V_{k+1} &= V_k + \mu_v R_{f,k}(G(V_{opt}^T R_{f,k}) - t_k - G(V_k^T R_{f,k})) \\ &= V_k + \mu_v R_{f,k}\left(\sum_i g_i\left((V_{opt}^T R_{f,k})^i - (V_k^T R_{f,k})^i\right) - t_k\right) \end{aligned} \tag{4.7}$$

Recalling that $a^i - b^i = (a-b)(a^{i-1} + a^{i-2}b + \ldots + b^{i-1})$ and defining the deviation vector $D_k = V_k - V_{opt}$, the behavior of the algorithm (4.3) can be described as:

$$D_{k+1} = (I - \mu_{v,k} R_{f,k} R_{f,k}^T) D_k - \mu_v R_{f,k} t_k \tag{4.8}$$

where $\mu_{v,k}$ is given by:

$$\mu_{v,k} = \mu_v \frac{G(V_k^T R_{f,k}) - G(V_{opt}^T R_{f,k})}{V_k^T R_{f,k} - V_{opt}^T R_{f,k}}$$

$$= \mu_v \begin{pmatrix} g_3\left((V_k^T R_{f,k})^2 + \ldots + (V_{opt}^T R_{f,k})^2\right) + \ldots \\ + g_{2N-1}\left((V_k^T R_{f,k})^{2N} + \ldots + (V_{opt}^T R_{f,k})^{2N}\right) \end{pmatrix} \quad (4.9)$$

From the Equation (4.8), we note that the proposed algorithm is an LMS algorithm with variable step size [34]. In order to analyze the convergence of this LMS-based algorithm, we will make the following additional assumptions:

Assumption 3: the truncation noise t_k is zero-mean and independent of $R_{f,k}$.

Assumption 4: $E(\mu_{v,k} R_{f,k} R_{f,k}^T D_k) = E(\mu_{v,k} R_{f,k} R_{f,k}^T) E(D_k)$

This assumption, known as the independence assumption, can be viewed as a good approximation for small step size.

Assumption 5: $F(r_k) = V_k^T R_{f,k} \in [0, A_s]$, *where* A_s *is the input amplitude that provides* $S \cdot P_{Sat}$ *at the output of the amplifier.*

This assumption is satisfied by setting $F(r_k) = min(A_s, V_k^T R_{f,k})$. It is worth noting that for $V_{opt}^T R_{f,k} \in [0, A_s]$, G is a C^∞ function, so one can conclude that there exists a real value $\gamma \in [0, A_s]$, such that

$$\mu_{v,k} = \mu_v G'(\gamma) \quad (4.10)$$

Recall that in the working area ($P_{max} < S \cdot P_{Sat}$), the function G is monotone and its derivative G' is a decreasing function ($0 \le G'(r) \le G'(0) = g_1$). It follows that

$0 \le \mu_{v,k} \le \mu_v g_1$

Using the above mentioned assumptions, one can establish the recurrence between $E(D_{k+1})$ and $E(D_k)$ by

$$E(D_{k+1}) = (I - E(\mu_{v,k} R_{f,k} R_{f,k}^T))E(D_k) \tag{4.11}$$

From Equation (4.11), one can determine the convergence conditions of the algorithm by

$$max\mu_{v,k} < \frac{2}{\lambda_{max} E(R_{f,k} R_{f,k}^T)} \tag{4.12}$$

where $\lambda_{max} E(R_{f,k} R_{f,k}^T)$ is the maximum eigenvalue of the matrix $E(R_{f,k} R_{f,k}^T)$

This condition leads to

$$\mu_v < \frac{2}{g_1 \lambda_{max} E(R_{f,k} R_{f,k}^T)} \tag{4.13}$$

Under the condition (4.13), the proposed algorithm converges to the optimum value. The convergence of the phase predistorter depends on the amplitude predistorter. When the condition (4.13) is satisfied, the optimum vector P_k converges to P_{opt} and the convergence analysis of the phase predistorter can be made. For small values of μ_ψ, we can use the independence assumption between the matrix $(I_{L+1} - \mu_\psi R_{\psi,k} R_{\psi,k}^T)$ and P_k, where I_{L+1} is the identity matrix with dimension $L+1$. Assuming n_k is a zero-mean process, the mean behavior of P_k can be described by

$$E(P_{k+1}) = (I_{L+1} - \mu_\psi E(R_{\psi,k} R_{\psi,k}^T))E(P_k) + \mu_\psi E(R_{\psi,k} R_{\psi,k}^T) P_{opt} \tag{4.14}$$

From Equation (4.14), the convergence of the phase predistorter to the optimal solution is guaranteed if the step size μ_ψ satisfies

$$\mu_\psi < \frac{2}{\lambda_{max} E(R_{\psi,k} R_{\psi,k}^T)} \tag{4.15}$$

If the conditions (4.13) and (4.15) hold, the proposed adaptive predistortion technique converges. Furthermore, for a given set of root-raised cosine (SRRC) filter, predistorter orders, correlation matrices $C_{R,v} = E(R_{f,k}R_{f,k}^T)$ and $C_{R,\psi} = E(R_{\psi,k}R_{\psi,k}^T)$, we can evaluate the rate of convergence.

Since the elements of vectors $R_{f,k}$ and $R_{\psi,k}$ represent the power of r, the eigenvalues of $C_{R,v}$ and $C_{R,\psi}$ are spreading. For a nonlinearity with order greater than 5, we can expect that:

$$\frac{\lambda_{min}(C_{R,v})}{\lambda_{max}(C_{R,v})} \ll 1, and \ \frac{\lambda_{min}(C_{R,\psi})}{\lambda_{max}(C_{R,\psi})} \ll 1 \tag{4.16}$$

This indicates a slow rate of convergence. Specifically, the coefficients of V_k and P_k, affecting the high power order of r, will exhibit a very long time to converge to the optimum values. These rates can be improved by introducing the matrices $\Gamma_v = C_{R,v}^{-(1/2)}$ and $\Gamma_\psi = C_{R,\psi}^{-(1/2)}$, in the adaptation of V_k and P_k:

$$\begin{aligned} V_{k+1} &= V_k + \mu_v \Gamma_v R_{f,k}(\delta r_k - G(V_k^T R_{f,k})) \\ P_{k+1} &= P_k + \mu_\psi e_{\psi,k} \Gamma_\psi R_{\psi,k} \end{aligned} \tag{4.17}$$

The algorithm given by Equation (4.17) is based on the self-orthogonalization adaptive technique [35]. For given modulation scheme, SRRC filter roll-off factor, and sampling frequency, we can evaluate $C_{R,v}$, $C_{R,\psi}$, Γ_v and Γ_ψ *off-line*, and use theses values in the adaptation procedure. This will increase the complexity, but provide better tracking capabilities. Compared to Equations (4.3),(4.5), the only difference in Equation (4.17) is the additional components Γ_v and Γ_ψ. Because Γ_v and Γ_ψ are computed off-line, they are considered as constants in this equation. Therefore, the additional complexity of the enhanced LMS-based algorithm given by Equation (38) is two constant matrix multiplications in comparison with the one of LMS-based algorithm given by Equations (4.3,4.5). If we consider the complexity of a constant multiplication and a real

multiplication is the same, and L is the length of the predistorter polynomial, then the complexity of the LMS based adaptive algorithm for the predistorter expressed in term of the number of multiplication is $2L + 1$, while the complexity of the enhanced LMS based adaptive algorithm is equal to $2L^2 + 2L + 1$.

The performance of the proposed predistorter evaluated by computer simulation will be discussed in the next section.

4.1.2. Performance Evaluation

The performances of the LMS-based and enhanced LMS-based algorithms are evaluated by simulation for a 64QAM system using a 7^{th}-order predistorter. The desired model (δ) is chosen to have $S = 0.950$, equivalent to $PBO = 0.22dB$.

Figures 4.1a-c show the evolution of V_k, P_k, and the normalized mean square error (MSE) of the LMS-based adaptive predistorter, respectively. The step sizes are $\mu_v = 0.5$, $\mu_\psi = 0.1$. The MSE between the desired and obtained models is defined as:

$$MSE = \frac{E(\left|\delta r - G(F(r))e^{j(\Phi(F(r)) + \Psi(r))}\right|^2)}{E(G(F(r))^2)} \tag{4.18}$$

The MSE is determined by running Monte-Carlo simulations over 200 sequences.

By investigating the behavior of V_k and P_k, it seems that the algorithm has an exponentially transient decrease, and the MSE converges to $-44dB$.

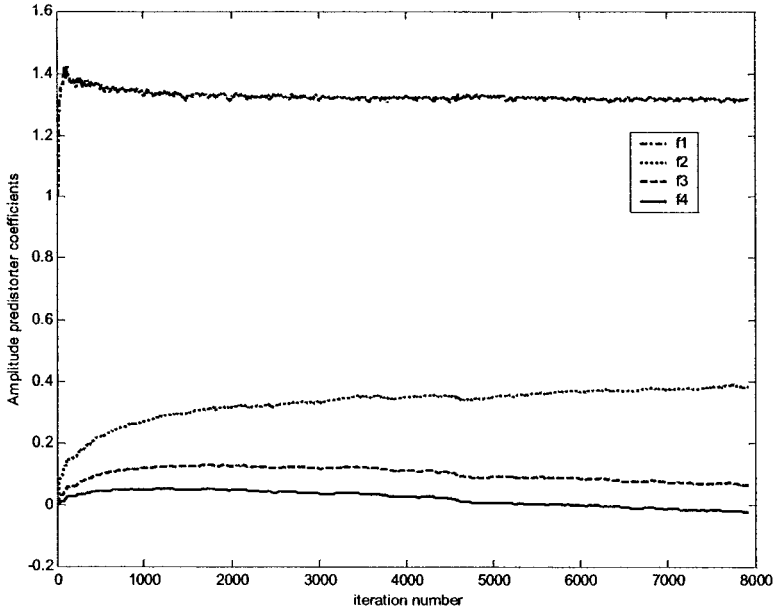

(a) Evolution of amplitude predistorter coefficients

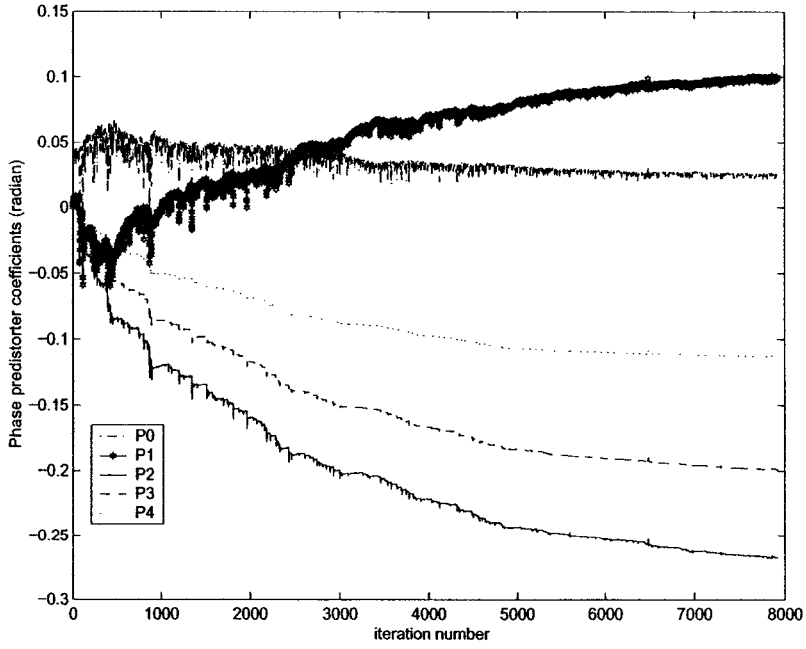

(b) Evolution of phase predistorter coefficients

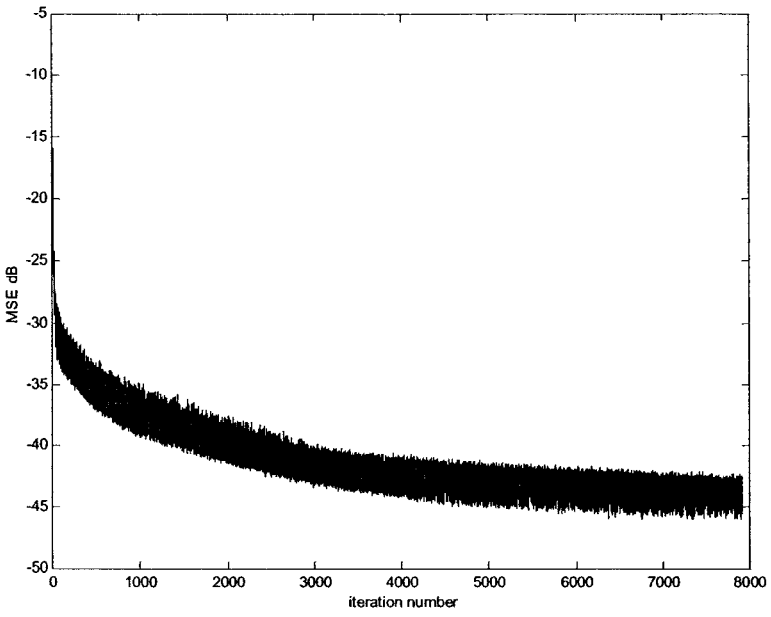

(c) Evolution of the MSE

Fig. 4.1: Behavior of the LMS-based algorithm (PBO=0.22dB)

The behavior of the enhanced LMS-based algorithm is depicted in Figure 4.2. The adaptation step sizes are $\mu_{\nu} = 0.05$, $\mu_{\psi} = 0.05$. The *MSE* of the enhanced LMS-based algorithm given by Eq. (4.17) converges to $-57dB$, which is smaller than that of LMS-based algorithm as expected. The LMS-based algorithm needs more time to converge to the global solution due to the spreading eigenvalues in the matrices $C_{R,\nu}$ and $C_{R,\psi}$. In practice, we can improve the rate of convergence by setting an initial condition V_0 close to the optimal one. However, due to its slow convergence, the LMS-based algorithm has a poor tracking capabilities.

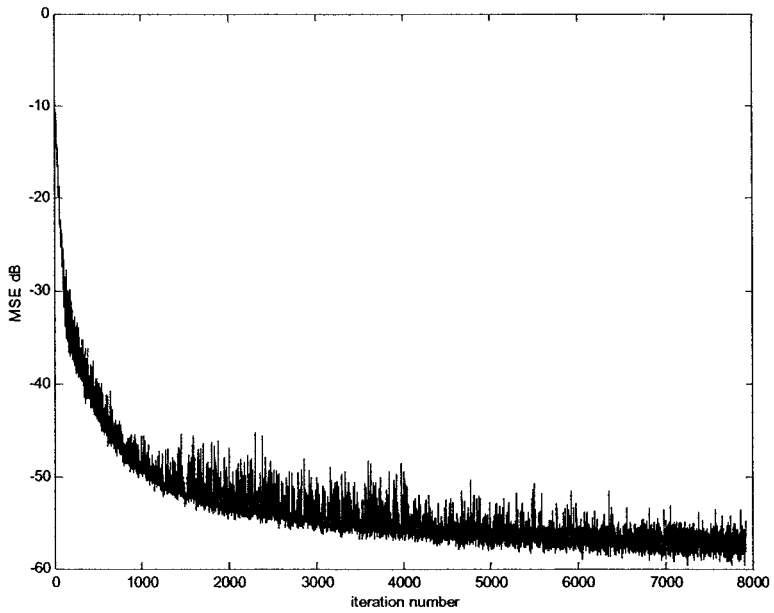

Fig. 4.2: Evolution of MSE of the enhanced LMS-based algorithm (PBO=0.22 dB)

In order to demonstrate the tracking capabilities of the proposed predistorter, we perturb the HPA characteristics by increasing the output power and phase shift by 10%. Figure 4.3 shows the evolution of the *MSE* for the LMS-based and enhanced LMS-based algorithms. The abrupt change occurs at iteration 100 (Figure 4.3). The MSE curve has a large value at 100 iteration, and is slowly reduced. It indicates that the algorithm can track the changes of the power amplifier. However, due to its slow convergence, the LMS-based algorithm takes longer time to converge to the new value after the change. The tracking capability can been improved when the enhanced LMS-based algorithm is used. It can be seen from the Figure 4.3, at the iteration 3000^{th}, the MSE of the LMS-based is about $-40dB$ while that of the enhanced LMS-based algorithm is below $-50dB$. In overall, after 100^{th} iteration, the MSE curve of enhanced LMS-based is steeper than that of LMS-based algorithm. This implies that the enhanced LMS-based algorithm has better tracking capability.

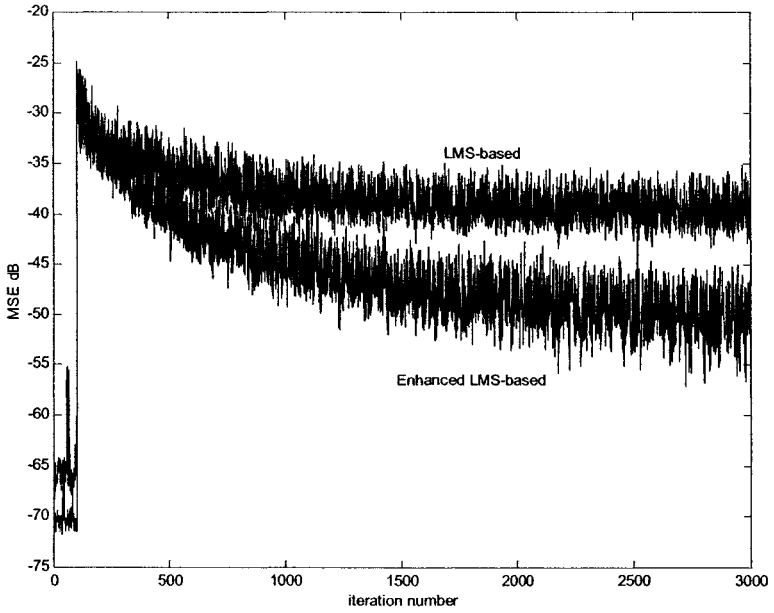

Fig. 4.3: Tracking capabilities of the LMS-based and enhanced LMS-based algorithms

4.2. RLS-based Algorithm

For a very fast convergence rate, we consider the RLS concept. In many cases, if a problem can be solved by using LMS based algorithm, a RLS based solution can also be derived. However, in this case, the function of the amplitude gain $G(.)$ and phase distorter $\Phi(.)$ of the power amplifier are not known at hand, it is not possible to derive the RLS based solution using cost functions similar to Equation (4.1). To remove $G(.)$ and $\Phi(.)$ in the error functions, we modify the input and output of the adaptive scheme as shown in Figure 4.4. The cost error function of the amplitude and phase are redefined

as:

$$J_1(V) = \varepsilon_f(n) = \sum_{i=1}^{n} \lambda_f^{n-i} |e_f(i)|^2$$
$$J_2(P) = \varepsilon_\psi(n) = \sum^{n} \lambda_\psi^{n-i} |e_\psi(i)|^2 \tag{4.19}$$

$$\begin{aligned}
\varepsilon_f(n) &= \sum_{i=1} \lambda_f^{n-i} |e_f(i)|^2 \\
&= \sum_{i=1}^{n} \lambda_f^{n-i} (r_{pd}(i) - V^T(n) R_{f,o}(i))^2 \\
&= \sum^{n} \lambda_f^{n-i} (r_{pd}^2(i) - 2 r_{pd}(i) V^T(n) R_{f,o}(i) + V^T(n) R_{f,o}(i) R_{f,o}(i)^T V(n))
\end{aligned} \tag{4.20}$$

where r_{pd} is the amplitude of the signal after the predistorter (input signal to the amplifier). $R_{f,o}$ is the input vector of the adaptation and is defined as $R_{f,o} = [r_{og}, r_{og}^3, r_{og}^5, \ldots, r_{og}^{2L-1}]^T$, where $r_{og} = \frac{r_o}{\delta}$, and r_o is the amplitude of the amplifier output signal. V is the coefficient vector of the amplitude gain predistorter function, and defined as $V = [f_1, f_3, \ldots f_{2L-1}]^T$.

Similarly, the error function of the phase predistorter is defined as

$$\begin{aligned}
\varepsilon_\psi(n) &= \sum_{i=1} \lambda_\psi^{n-i} |e_\psi(i)|^2 \\
&= \sum_{i=1}^{n} \lambda_\psi^{n-i} (P^T(n) R_{\psi,o}(i) + \theta_d(n))^2 \\
&= \sum^{n} \lambda_\psi^{n-i} (P^T(n) R_{\psi,o}(i) R_{\psi,o}^T(i) P(n) + 2\theta_d(n) P^T(n) R_{\psi,o}(i) + \theta_d^2(n))
\end{aligned} \tag{4.21}$$

where θ_d is the distorted phase produced by the power amplifier, and $\theta_d = \theta_o - \psi_{pd}$.

θ_o is the phase of the amplifier output signal, ψ_{pd} is the sum of the input signal phase and the predistorted phase. $R_{\psi,o}$ is the input vector of the adaptive phase predistorter and defined as $R_{\psi,o} = [1, r_{pd}, r_{pd}^3, r_{pd}^5, \ldots, r_{pd}^{2K-1}]^T$, where r_{pd} is the amplitude of the output signal of the predistorter (or the amplitude of the input signal to the amplifier). $P(n)$ is the coefficient vector of the phase predistorter at iteration n, and defined as $P = [\psi_0, \psi_1, \psi_3, \ldots, \psi_{2K-1}]^T$

Taking the gradient of $\varepsilon_f(n)$ with respect to V and $\varepsilon_\psi(n)$ with respect to P, we obtain

$$\nabla_V \varepsilon_f(n) = \sum_{i=1}^{n} \lambda_f^{n-i}(2R_{f,o}(i)R_{f,o}(i)^T V(n) - 2R_{f,o}(i)r_{pd}(i))) \tag{4.22}$$

$$\nabla_P \varepsilon_\psi(n) = \sum_{i=1}^{n} \lambda_\psi^{n-i}(2R_{\psi,o}(i)R_{\psi,o}(i)^T P(n) + 2R_{\psi,o}(i)\theta_d(i)) \tag{4.23}$$

The tap-weight vector $V(n)$ reaches its optimum value, corresponding to the minimum value of the cost function $\varepsilon_f(n)$ of Eq. (4.20) when $\nabla_V \varepsilon_f(n) = 0$. Therefore, from Equation (4.22), we obtain,

$$\left[\sum_{i=1}^{n} \lambda_f^{n-i} R_{f,o}(i)R_{f,o}(i)^T\right] V(n) = \sum_{i=1}^{n} \lambda_f^{n-i} R_{f,o}(i)r_{pd}(i) \tag{4.24}$$

or

$$Q_f(n)V(n) = Z(n) \tag{4.25}$$

where

$$\begin{aligned} Q_f(n) &= \sum_{i=1}^{n} \lambda_f^{n-i} R_{f,o}(i)R_{f,o}(i)^T \\ Z(n) &= \sum_{n} \lambda_f^{n-i} R_{f,o}(i)r_{pd}(i) \end{aligned} \tag{4.26}$$

Assume that $Q_f(n)$ is positive definite and therefore nonsingular. Applying RLS algorithm [33] to Equation (4.25), we obtain the following recursive equations,

$$\begin{aligned} k_f(n) &= \frac{\lambda_f^{-1} Q_f(n-1) R_{f,o}(n)}{1+\lambda^{-1} R_{f,o}^T(n) Q_f(n-1) R_{f,o}(n)} \\ \varepsilon_f(n) &= r_{pd}(n) - V^T(n-1) R_{f,o}(n) \\ V(n) &= V(n-1) + k_f(n)\varepsilon_f(n) \\ Q_f(n) &= \lambda_f^{-1} Q_f(n-1) - \lambda_f^{-1} k_f(n) R_{f,o}^T(n) Q_f(n-1) \end{aligned} \tag{4.27}$$

with

$$\begin{aligned} Q_f(0) &= \delta_f^{-1} I \\ V(0) &= \text{an arbitrary nonzero vector} \end{aligned}$$

Similarly, we can derive the following recursive equations for the phase,

$$\begin{aligned} k_\psi(n) &= \frac{\lambda_\psi^{-1} Q_\psi(n-1) R_{\psi,o}(n)}{1+\lambda^{-1} R_{\psi,o}^T(n) Q_\psi(n-1) R_{\psi,o}(n)} \\ \varepsilon_\psi(n) &= \theta_d(n) + P^T(n-1) R_{\psi,o}(n) \\ P(n) &= P(n-1) - k_\psi(n)\varepsilon_\psi(n) \\ Q_\psi(n) &= \lambda_\psi^{-1} Q_\psi(n-1) - \lambda_\psi^{-1} k_\psi(n) R_{\psi,o}^T(n) Q_\psi(n-1) \end{aligned} \tag{4.28}$$

with

$$\begin{aligned} Q_\psi(0) &= \delta_\psi^{-1} I \\ P(0) &= \text{an arbitrary nonzero vector} \end{aligned}$$

When the amplitude adaptive equation converges, $V = V_{opt}$ and $\varepsilon_f(n) = 0$. Therefore, from Equation (4.27), we obtain

$$V_{opt} R_{f,o}(n) = r_{pd}(n)$$

or

$$F(r_{og}) = r_{pd}$$

The amplitude of the amplifier output is

$$G(r_{pd}) = r_o$$

or $$G(F(r_{og})) = G(F(r_o/\delta)) = r_o$$

Therefore,

$$G(F(r(t))) = \delta r(t)$$

which satisfies the amplitude equation expressed in (3.5).

Similarly, when the phase adaptive algorithm converges, then $P = P_{opt}$ and $\varepsilon_{\psi}(n) = 0$. From Equation (4.28), we obtain

$$\theta_d + P_{opt}^T R_{\psi, o}(n) = 0$$

or

$$\Phi(V_{opt}^T R_{\psi, o}(n)) + P_{opt}^T R_{\psi, o}(n) = 0 \tag{4.29}$$

We can rewrite Equation (4.29) as

$$\Phi(F(r(t))) + \Psi(r(t)) = 0 \tag{4.30}$$

which also satisfies the requirement of the phase predistorter given by Equation (3.5).

In summary, we have shown that the proposed RLS-based algorithm produces the amplitude and phase functions that meet the requirement of the predistorter in compensating the distortion introduced by the power amplifier.

The performance of the predistorter system using RLS-based adaptive algorithm given in (4.27) and (4.28) is shown in Figure 4.5. In simulation, the predistorter order is set to 7 ($L = K = 4$). The power amplifier model is the same used in [22]. The peak power backoff (PBO) is set to $2dB$ and the transmitted signal is 16QAM. The value of forgetting factor (λ) is always set to 1. Note that we have used all the same system parameters as in [22] to make the comparison easier.

Figure 4.5 shows the spectra of the transmitted 16QAM signal with the root raised cosine filter roll-off factor of 0.5 at various iterations, n. In this figure, the linear case corresponds to distortionless signal. The signal spectrum without the predistorter has a very high out-of-band level in the case of $PBO = 2dB$. As the number of iteration

increases, the out-of-band level is reduced. After 30 iterations, the out-of-band level is significantly reduced (below $-80dB$) and the improvement is more than $50dB$ compared with the case of there is no predistorter. The similar result was reported in [22] requires about 50 iterations. This indicates that the proposed technique converges faster than the one proposed in [22].

There are $4L^2+3L$ and $4K^2+11K+7$ multiplications are used in the recursive equations of the amplitude and phase predistorters respectively. For the case of $L = K$, the total complexity of the RLS adaptive algorithm for the predistorter, expressed in term of the number of mulitplication, is $8L^2+14L+7$.

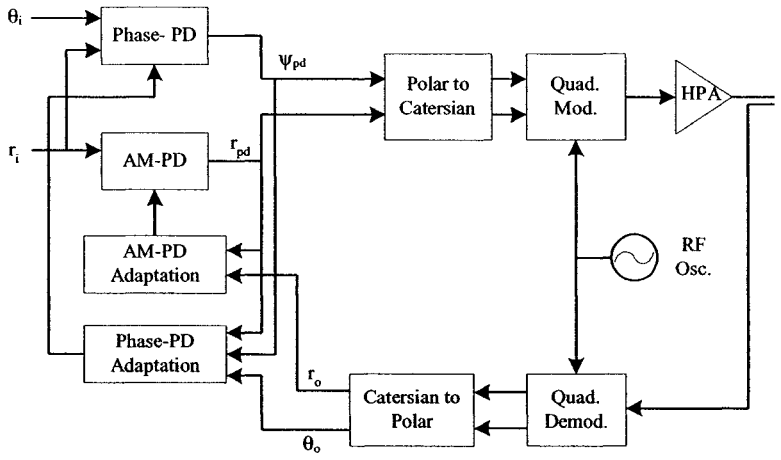

Fig. 4.4: RLS adaptive predistorter

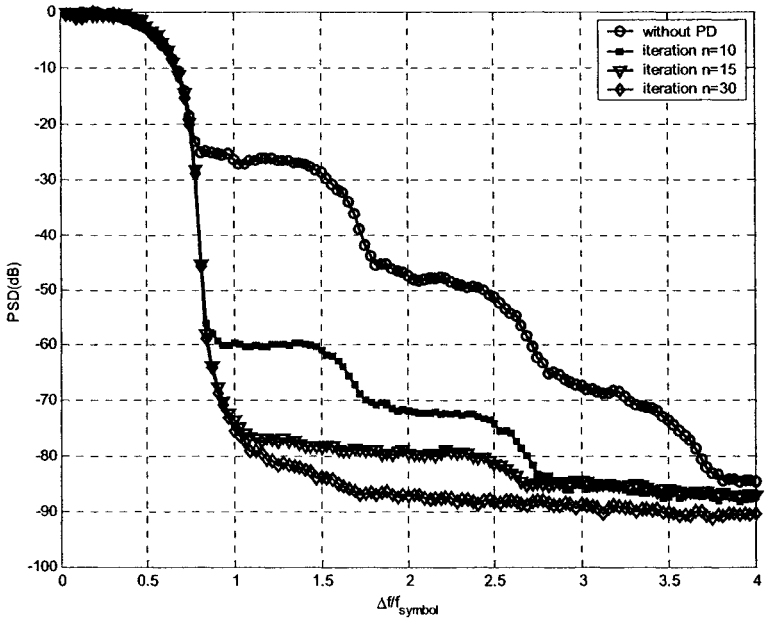

Fig. 4.5: Power spectra of 16QAM signal with and without the RLS predistorter

4.2.1. Simplified Structure

The complexity of the RLS algorithm presented in (4.27) and (4.28) depends on the computation of $k(n)$ and $Q(n)$ in the recursive equations. The error and weight updating equations have much lower complexity. In the proposed scheme, we need both amplitude and phase predistortion functions corresponding to two separated RLS adaptive blocks. However, the recursive equations of $k(n)$ and $Q(n)$ depend only on the values of λ and $R(n)$. If we can make $\lambda_f = \lambda_\psi$ and $R_{\psi,o}(n) = R_{f,o}(n)$, then $k_f(n)$, $Q_f(n)$ and $k_\psi(n)$, $Q_\psi(n)$ are identical in each iteration. As the result, instead of computing $k_f(n)$, $Q_f(n)$, $k_\psi(n)$, $Q_\psi(n)$ separately in each iteration, we need to compute only one of two pairs. Therefore, the complexity of the adaptive block of the predistorter is reduced approximately by half. The cost functions of the amplitude gain and phase predistorter

adaptive algorithm are redefined as,

$$\varepsilon_f(n) = \sum_{i=1}^{n} \lambda_f^{n-i} \left| e_f(i) \right|^2 = \sum_{i=1}^{n} \lambda_f^{n-i} \left(r_{pd}(i) - V^T(n) R_o(i) \right)^2 \tag{4.31}$$

$$\varepsilon_\psi(n) = \sum_{i=1}^{n} \lambda_\psi^{n-i} \left| e_\psi(i) \right|^2 = \sum_{i=1}^{n} \lambda_\psi^{n-i} \left(\theta_d(n) + P^T(n) R_o(i) \right)^2 \tag{4.32}$$

The recursive equations now can be rewritten as,

$$\begin{aligned} k(n) &= \frac{\lambda^{-1} Q(n-1) R_o(n)}{1 + \lambda^{-1} R_o^T(n) Q(n-1) R_o(n)} \\ \varepsilon_f(n) &= r_{pd} - V^T(n-1) R_o(n) \\ \varepsilon_\psi(n) &= \theta_d(n) + P^T(n-1) R_o(n) \\ V(n) &= V(n-1) - k(n) \varepsilon_f(n) \\ P(n) &= P(n-1) - k(n) \varepsilon_\psi(n) \\ Q(n) &= \lambda^{-1} Q(n-1) - \lambda^{-1} k(n) R_o^T(n) Q(n-1) \end{aligned} \tag{4.33}$$

The structure of this simplified RLS algorithm is shown in Figure 4.6 and its performance is shown in Figure 4.7. From the Equation (4.33), we can easily calculate the complexity of this algorithm and it is equal to $4L^2 + 13L + 7$ (assume $L = K$). The simplified RLS adaptive algorithm has the same convergence rate of the RLS algorithm discussed in the previous section. An improvement of more than $50dB$ in the out-of-band level can be obtained only after 30 iterations. This technique uses only one set of recursive equations and two polynomial functions (for phase and amplitude), while the fast algorithm proposed in [22] requires one set of recursive equations, one update predistorter coefficient block and four polynomial functions (I and Q for pre and post-distorter). In summary, the complexity of the adaptive algorithm given by [22] is higher than that of the proposed simplified RLS based algorithm by the update predistorter coefficient block. Because each predistorter coefficient in the update predistorter coefficient block of the algorithm in [22] is expressed as a polynomial of the cosine of the

phase shift, this block alone uses $2L^2 + 2L$ multiplications. Therefore, the structure we propose has smaller complexity than what proposed in [22] by $2L^2 + 2L$ multiplications, it also provides faster convergence rate.

All the simulations were running on a floating point platform. We also note that RLS is well known for its fast convergence rate; however there is a numerical instability problem to be considered when RLS algorithm is implemented in finite-precision arithmetic [33]. For this reason, in practice, an RLS algorithm is often used only at the beginning to reduce the training time. Once the algorithm converges, a LMS will replace the RLS algorithm for its low complexity and more stable due to the roundoff noise.

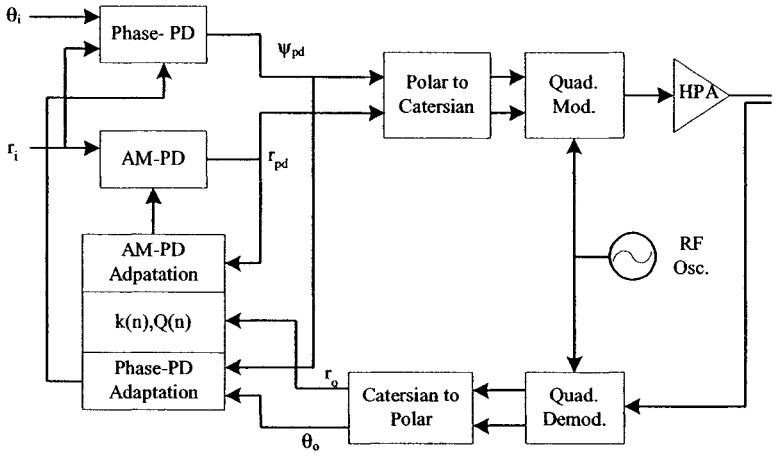

Fig. 4.6: Simplified RLS adaptive predistorter

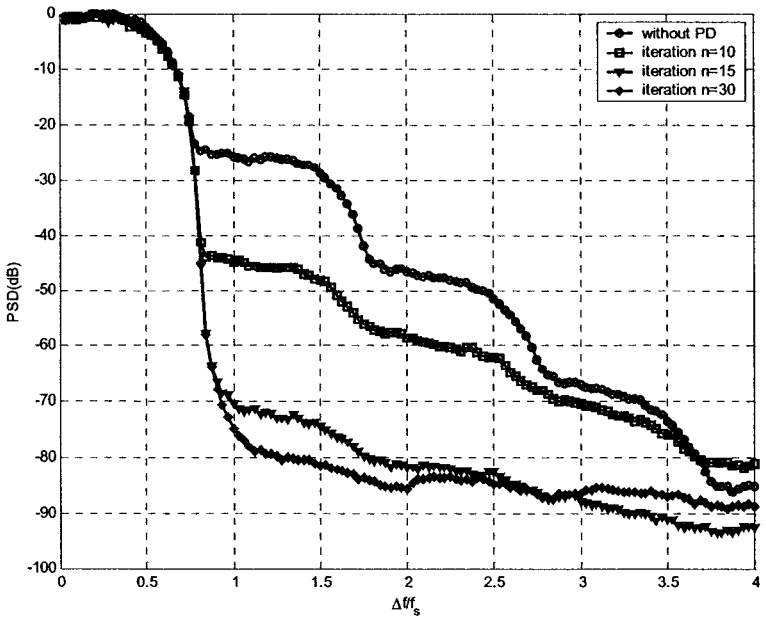

Fig. 4.7: Power spectra of filter 16QAM signal with and without the simplified RLS adaptive predistorter

4.2.2. Cascaded Structure

The convergence rate can be improved if we modify the phase error function so that it does not depend on the convergence of the amplitude gain adaptive algorithm. This modified structure (cascaded structure) is shown in Figure 4.8.

Instead of the amplitude $r(t)$, we pass the output of the amplitude predistorter, $F(r(t))$, to the phase predistorter. The phase predistorter equation is rewritten as

$$\Phi(F(r(t))) + \Psi(F(r(t))) = 0 \tag{4.34}$$

The phase predistorter now operates independently of the convergence of the amplitude gain predistorter function. The cost functions of the amplitude gain and phase predistorter adaptive algorithms remain unchanged. Hence, there is no change in the

recursive equations except for the input vector of the phase predistorter function.

The signal spectra in different iterations plotted in Figure 4.9 show the improvement in convergence rate of the cascaded structure: An out-of-band level below $-80dB$ can be achieved with only 20 iterations. For the RLS and simplified RLS adaptive algorithms, similar result can be obtain only after 30 iterations. This improvement is possible because the predistorter phase and amplitude adaptive processes converge simultaneously at the same time and independently of each other. While in the previously discussed RLS and simplified RLS techniques, the phase predistorter adaptive process depends on the amplitude and therefore converges only after the amplitude has converged.

The main disadvantage of this technique is that it has higher complexity (almost two times) comparing with the simplified RLS predistorter.

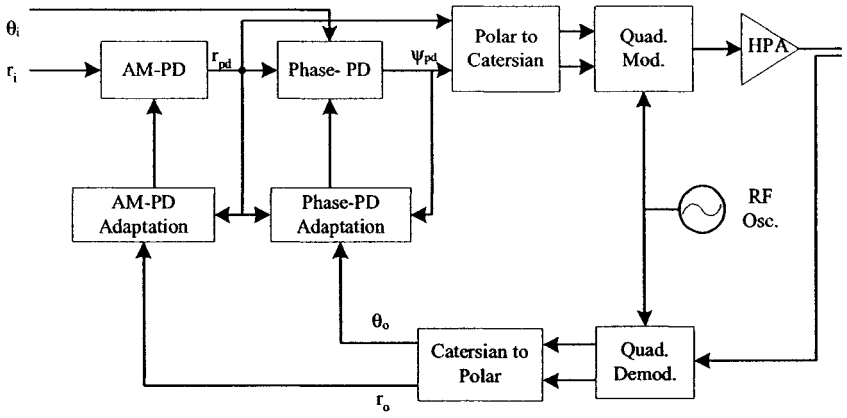

Fig. 4.8: RLS cascaded adaptive predistorter

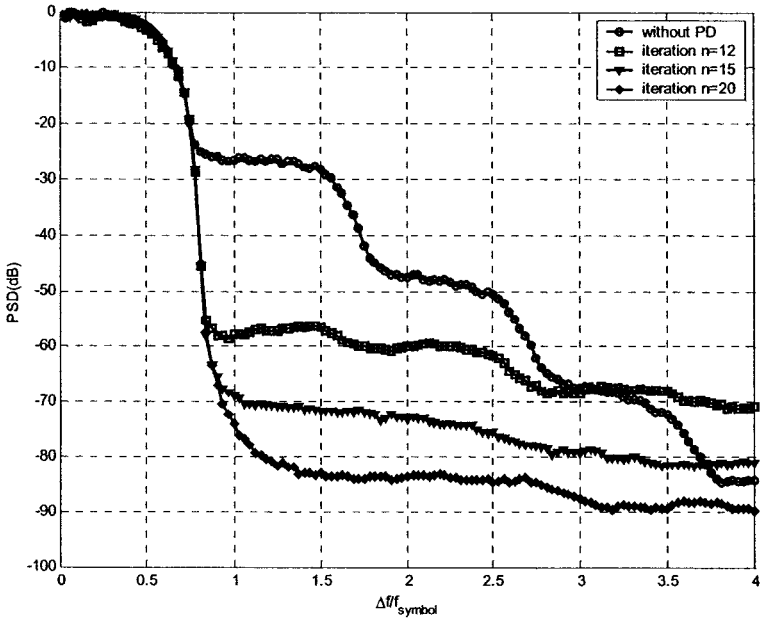

Fig. 4.9: Power spectra of filter 16QAM signal with and without the RLS cascaded adaptive predistorter

Chapter 5. Power and Bandwidth-Efficient Circular M-ary APK Schemes with low PAR

In the past, there has been a number of studies on signalling constellations for high performance. Kernighan and Lin [36] suggested an algorithm to search for good constellations to minimize the average error rate under a specified noise condition, using a maximum-likelihood decoding scheme. To reduce the complexity of the optimal signal design problem, their approach is to discretize the two-dimensional space under a peak power constraint so that the problem can be formulated, programmed and solved on computer. Their reported optimal circular (5,11) APK constellation in an additive white Gaussian noise (AWGN) environment has been verified in [37, 38, 39]. An in-depth investigation of M-ary APK constellations in [37] determined optimum designs for M = 4 to 128 in terms of symbol error probability bound for both average and peak SNR. Blyth and Jones [40] proposed a method to design signal constellation based on hypercubes. An iterative approach using polar quantization to design the signal constellation with optimization criterion based on the quantization mean square error (MSE) [41] resulted in an optimum 256-APK. Dabak and Johnson [42] proposed a new method for designing signal constellations for non-Gaussian environment using geometry structure for detection theory. In general, these studies focused on the minimum distance or SNR.

For systems using non-linear amplifiers, treating the *squared minimum distance to average power ratio* (DPR) and the *peak to average power ratio* (PAR) *separately* does not guarantee the optimum performance since a high DPR can offer a better detection

performance but might imply also a high PAR and, consequently, require high output back-off (OBO) of the power amplifier or poor transmit power efficiency.

5.1. Peak to Average Power Ratio (PAR) Consideration

Consider a M-ary APK transmitter shown in Figure 5.1.

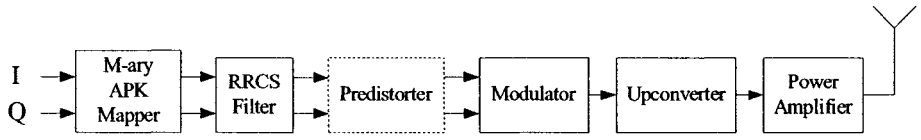

Fig. 5.1: Basic block diagram of a M-ary APK transmitter

Root raised-cosine filters (RRCS) are used for bandlimited transmission. The complex baseband pre-distorter is an optional block used to compensate the AM/AM and AM/PM distortion of the transmit power amplifier (PA) when the PA operates near saturation for its highest power efficiency. Various reported pre-distortion techniques [15, 18, 24] indicate that the PA with predistorter can operate with the *peak* signal power extremely close to saturation, i.e., the *peak* backoff (PBO) of the PA is close to $0dB$ (e.g., around $0.2dB$). It follows that the *average* output backoff (OBO) of the PA can be expressed as the sum of the PBO and PAR in dB. Since the OBO represents the loss in power efficiency and PBO is close to $0dB$, the peak-to-average power ratio (PAR) of the filtered modulated signal is the dominant factor in determining the transmitter power efficiency. For this, it is desired to keep a filtered modulated signal with low PAR.

5.2. Effects of Filtering on PAR

We consider digital signal processing applied to the baseband signals, i.e., signals are processed as discrete-time samples. The output of the spectrum shaping filter can be

written as,

$$y(kT_s) = \sum_{n=-\infty}^{\infty} x_u(nT_s)h((k-n)T_s) \tag{5.1}$$

where $y(\ )$ is the output signal, $x_u(\ )$ is the input signal and $h(\ )$ is the impulse response of the spectrum shaping filter, and T_s is the sampling frequency. Without confusion and for simplicity, we drop T_s from the equation, i.e., Equation (5.1) becomes

$$y[k] = \sum_{n=-\infty}^{\infty} x_u[n]h[k-n] \tag{5.2}$$

It is often chosen that $T_{symbol}/T_s = M$, where T_{symbol} is the symbol period and M is an integer greater than 1, i.e., the M-ary ASK symbols are up-sampled to produce $x_u[n]$. In the m^{th} symbol interval mT_{symbol}, among M samples $x_u[n]$ where $n = mM + i$ and $i = 0, 1, 2, \ldots, M-1$, we need only one to represent the M-ary ASK symbol $x[mT_{symbol}]$. Therefore,

$$x_u[n] = \begin{cases} x[mT_{symbol}], & n = mM \\ 0 & \text{otherwise} \end{cases} \tag{5.3}$$

It follows that,

$$y[k] = \sum_{m=-\infty}^{\infty} x[m]h[k-mM] \tag{5.4}$$

The peak value of $y[k]$ is approximately

$$|y|_{max} \le |x_p| \sum_{n=-\infty}^{\infty} |h[k_o - mM]| \tag{5.5}$$

where k_o is a selected value of k $(0 \le k_o < M)$ such as the factor $\sum_{n=-\infty}^{\infty} |h[k_o - mM]|$ is

maximized, $|x_p|$ is the amplitude of the peak symbol of the complex-valued symbol sequence $x[n]$. For a zero-mean symbol sequence, the above relation becomes an equality if the constellation contains antipodal peak symbols x_p and $-x_p$, which is the case for symmetric constellations.

Equation (5.5) indicates that the peak amplitude of the signal at the spectrum shaping filter output is the product of the symbol peak amplitude and a factor β,

$$\beta = \sum_n |h[k_o - nM]| \tag{5.6}$$

representing the filter effects. It follows that

$$P_{\text{peak\_out}} = P_{\text{peak\_symbol}} + 20\log\beta \tag{5.7}$$

where $P_{\text{peak\_out}}$ and $P_{\text{peak\_symbol}}$ are the peak power (in dBm) of the filter output signal and input symbol, respectively.

Consider a root raised-cosine filter (RRCS) [25] used for spectrum shaping, which is the common case for bandlimited signals. Figure 5.2 shows the value of β as a function of the filter rolloff factor α and the offset k_o with the upsampling factor $M = 16$. The bold line shows the maximum values β corresponding to different values of the filter roll-off factor, α.

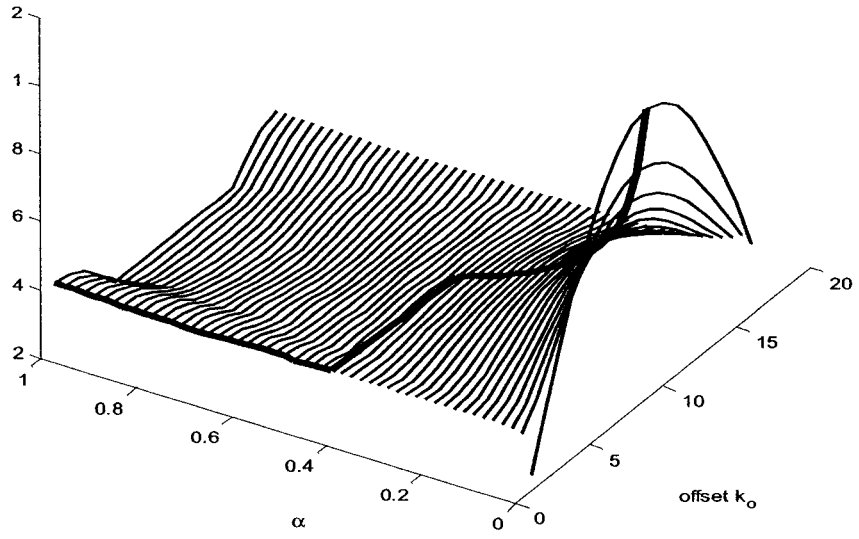

Fig. 5.2: β as a function of α and offset k_o

The power spectral density of the output signal of the spectrum shaping filter is,

$$S_y(f) = S_x(f)|H(f)|^2 \tag{5.8}$$

where $S_x(f)$ is the power density spectrum of the input signal and $H(f)$ is the discrete transfer function of the spectrum shaping filter. For RRCS spectrum shaping filter, from the Nyquist's criterion [25],

$$|H(f)|^2 = \frac{1}{T_s} \sum_{k=-\infty}^{\infty} X_{rc}(f - kf_s) = 1 \tag{5.9}$$

where

$$X_{rc}(f) = \begin{cases} T_s & \left(0 \le |f| \le \frac{1-\alpha}{2T_s}\right) \\ \frac{T_s}{2}\left\{1 + \cos\left[\frac{\pi T_s}{\alpha}\left(|f| - \frac{1-\alpha}{2T_s}\right)\right]\right\} & \left(\frac{1-\alpha}{2T_s} \le |f| \le \frac{1+\alpha}{2T_s}\right) \\ 0 & \left(|f| > \frac{1+\alpha}{2T_s}\right) \end{cases} \tag{5.10}$$

Therefore,

$$S_y(f) = S_x(f) \tag{5.11}$$

The above equation implies that the input and output signals of the RRCS shaping filter have the same *average* power. From equations (5.7) and (5.11), for a RRCS shaping filter, we obtain

$$PAR_{\text{out}} = PAR_{\text{symbol}} + 20\log\beta \tag{5.12}$$

where PAR_{out} and $\text{PAR}_{\text{symbol}}$ are the peak-to-average power ratios (in dB) of the RRCS filter output signal and input symbol, respectively.

5.3. Optimum criterion for M-ary APK constellation for nonlinear amplification

Consider the M-ary transmission in an additive white Gaussian noise (AWGN) environment. It is well known that a constellation with a larger minimum distance yields a better *receiver* performance in terms of error probability [25]. However, a larger minimum distance may imply a larger *average* power requirement. Therefore, taking into account the power efficiency, a good constellation must have a high squared- minimum-distance-to-average-power ratio (DPR).

On the other hand, the power efficiency of the *transmit* power amplifier can be

represented by

$$\varepsilon_T = \frac{P_T}{P_{DC}} = \frac{P_T}{P_{sat}} \frac{P_{sat}}{P_{DC}} \tag{5.13}$$

where P_T, P_{sat}, and P_{DC} are the average transmitted power, saturated power and supply power, respectively. The ratio $\frac{P_{sat}}{P_{DC}}$ is determined by the amplifier design technique and technology while the ratio $\frac{P_T}{P_{sat}}$ is related to the required average output backoff (OBO) in dB as $OBO = PBO + PAR = -10log_{10}\left(\frac{P_T}{P_{sat}}\right)$. The peak output backoff (PBO) and PAR are expressed in dB.

The above relations indicates that a transmitted M-ary APK signal with low PAR allows the power amplifier to operate at low OBO for high power efficiency.

In consideration of the power efficiency of the overall system, it is desired to design the M-ary APK constellations with the highest DPR and lowest PAR. Introducing the *normalized* average power, $\bar{P}_{ave}$, defined as the ratio of the average power to the squared minimum distance, it is obvious that $\bar{P}_{ave} = \frac{1}{DPR}$. The design objective can be represented as an optimization problem to minimize the following cost function:

$$W = \bar{P}_{ave} + PAR_{symbol} \tag{5.14}$$

where PAR_{symbol} (in dB) represents the peak-to-average power ratio of the M-ary APK constellation. Both W and $\bar{P}_{ave}$ are also expressed in dB.

5.4. Best Circular M-ary APK Constellations

Based on the above defined cost function W, we developed an optimal constellation

search algorithm and searched for a number of best circular M-ary APK constellations

5.4.1. Optimal Constellation Search Algorithm

We consider circular constellations for their general PAR requirement [36,40,39]. Furthermore, for simplicity, we limit the optimum search to circular constellation with the following characteristics:

a) Constellation has elements on concentric circles.

b) The elements on the same circle are equally spaced.

c) Number of elements on the outer circle is equal or greater than that on the inner circle.

d) Except the center, number of elements on a circle is greater than 1.

The proposed algorithm is based on exhausted search. However, the number of search case is reduced due to the above rules. The rules a) and b) narrow the possibility of the points on the IQ plane, which simplify in formulating the search problem. The rules c) and d) are needed to early eliminate the cases that are not possible to lead to the optimal constellations, which will reduce the search time. The search will start first with the set of one level (one circle), then it goes on to the case of two levels, three levels, etc... until M levels have been reached. The constellation has the smallest weight among these cases will be the optimal one for M-APK signaling scheme. For every set of k levels, the total number of points M will be placed on the k circles without violating the rules discussed above. The radii of the circles are also adjusted such as the minimum distance between two points on the constellation is not smaller than a constant d_{min} and the average power is minimized. The pseudo-code of the algorithm is given below:

// Main program

1. *Initialize current best set S_c to NULL.*
2. *Initialize the current best weight W_c to ∞.*
3. *Initialize the level l to 1.*
4. *If l is equal to $M/2$ go to step 11, otherwise go to the next step.*
5. *Initialize the S_l to NULL and W_l to ∞.*
6. *Call Recursive_Level_Search(l) function to find the best candidate for the set having l level (W_l and S_l represent the weight and the set found respectively).*

7. *If the W_l is larger or equal to the current best weight W_c, go to step 9, otherwise go to the next step.*
8. *Set S_c to S_l and W_c to W_l.*
9. *Increment l.*
10. *Go to step 4.*
11. *Report the the best set S_c*
12. *End main program.*

// Recursive_Level_Search(current_level) function

13. *If current_level is equal to 1, go to step 21, otherwise go to the next step.*
14. *Compute the maximum number of point allowed for this level (max_nb_cur).*
15. *Set the max_nb_point to the minimum of max_nb_cur and the number of point allocated for the level of current_level+1.*
16. *Initialize i to 2.*
17. *If i is equal to max_nb_point, go to step 22, otherwise go to the next step.*
18. *Call Recursive_Level_Search($i+1$) function.*
19. *Increment i.*
20. *Go to step 17.*
21. *Compute the number of point of this level (the innermost level): nb_point.*
22. *If nb_point is greater than 10, go to step 27, otherwise go to the next step.*
23. *If nb_point is greater than the number of point allocated for the level of (current_level+1) go to 27, otherwise go to the next step.*
24. *Call N_level() function to arrange the set constellation for a smallest weight W_i, corresponding with the set S_i.*
25. *If the W_i is larger or equal to the current best weight W_l, go to step 27, otherwise go to the next step. (S_l is the current best set and its weight is denoted as W_l for level l)*
26. *Set S_l toS_i and W_l to W_i.*
27. *End of Recursive_Level_Search function.*

// N_level() function

28. *Initialize i to 1.*
29. *If i is equal to the highest level+1, go to step 38.*
30. *Calculate the smallest radius r_d with respect to the minimum distance. D_MIN given number of point of the level i^{th}.*
31. *If r_d is greater or equal to the radius of the inner circle (r_{i-1}) plus D_MIN, go to step 35, otherwise go to the next step.*
32. *Rotate the points (placed symmetrical on the circle) until the smallest radius r_m is found ($r_m \le r_{i-1} + \text{D\_MIN}$).*
33. *Set r_i to r_m.*
34. *Go to step 36.*
35. *Set r_i to r_d.*
36. *Increment i*

37. Go to step 29
38. End of function N_level

5.5. Optimal constellations for 8-,16-,32-,64-,128-APK schemes

Using the search algorithm presented in the previous section, we searched for M-ary APK constellations with M=8, 16, 32, 64, 128. The case of M=4 is trivial as the classical 4PSK (or 4QAM) constellation is the best one.

5.5.1. Circular (7,1)APK

With M=8, the number of concentric circles can be up to 4. The best constellation denoted as (7,1)APK, has one element at the center and seven on one circle as shown in Figure 5.4. Table 5.1 summarizes the normalized average power and the peak to average power ratio. The performance of this (7,1)APK is compared with that of the popular (4,4)APK shown in Figure 5.3. The result represented by the difference between the values of the weight indicates an overall improvement of 1.48dB. Note that the (4,4)APK constellation was found in the search was already eliminated since the (7,1)APK has a better performance.

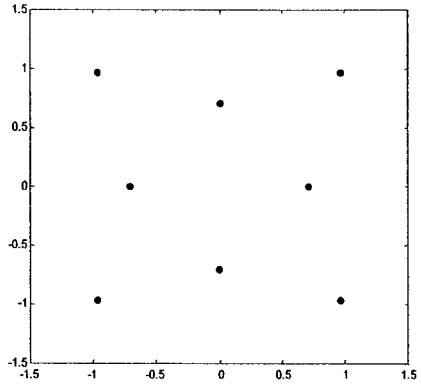

Fig. 5.3: (4,4)APK constellation

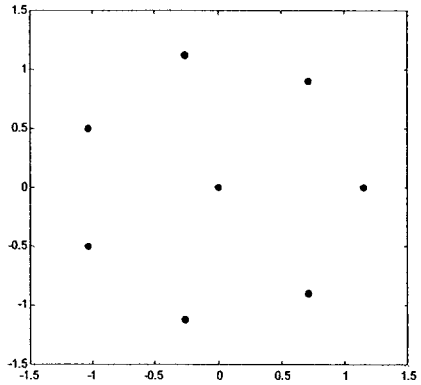

Fig. 5.4: (7,1)APK constellation

Constellation set	$\bar{P}_{ave}$(dB)	PAR (dB)	W(dB)
(4,4)APK	0.73	1.98	2.71
(7,1)APK	0.65	0.58	1.23

Table 5.1: Performance comparison between (4,4)APK and (7,1)APK constellations

In the search algorithm, the union bound is used for simple and fast calculation of the weight W. We also use simulation to evaluate the symbol error rate performance of the two constellation sets for verification. The simulation result in Figure 5.5 shows that the advantage in the normalized average power of the (7,1)APK over the (4,4)APK constellation is 0.39dB, instead of 0.08dB obtained from the union bound. Therefore, the overall gain of the (7,1)APK over the (4,4)APK is 1.79 dB.

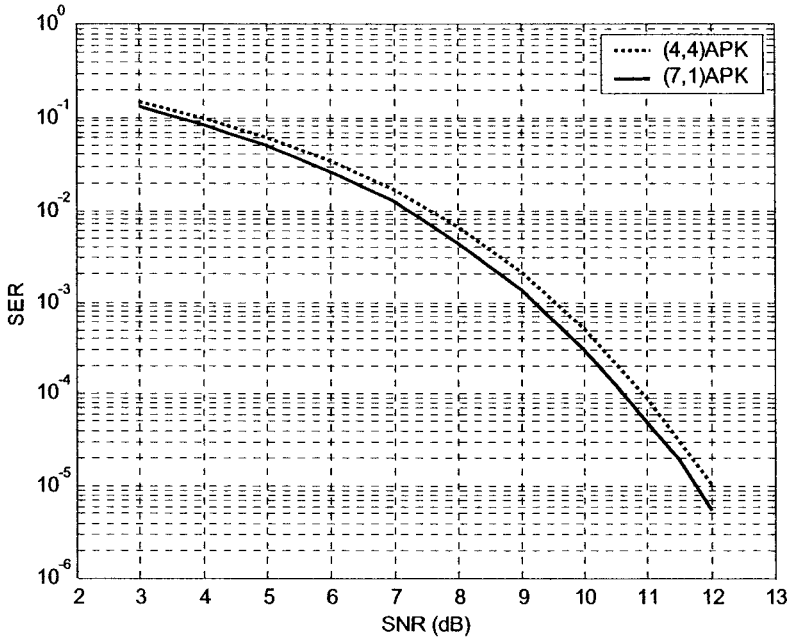

Fig. 5.5: Symbol error rate of (4,4)APK and (7,1)APK

5.5.2. Circular (11,5)APK

For M=16, the obtained optimum constellation, (11,5)APK, has 11 elements on the outer circle and 5 on the inner circle as depicted in Figure 5.7. Kernighan and Lin [36] also found this (11,5)APK constellation to be optimal in AWGN environment. The performance of this (11,5)APK is compared to that of the popular square 16QAM (Figure 5.6). Results summarized in Table 5.2 show the (11,5)APK has slightly higher normalized average power but lower peak to average power ratio than the square 16QAM. The overall weight W indicates an overall gain provided by the (11,5)APK of about 1.19dB.

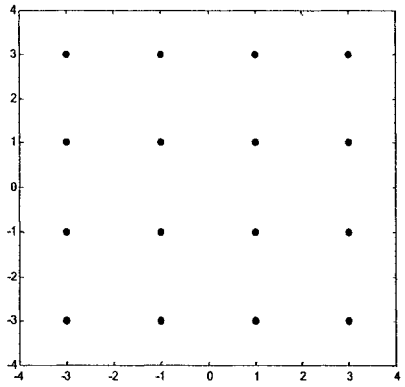

Fig. 5.6: Square 16QAM constellation

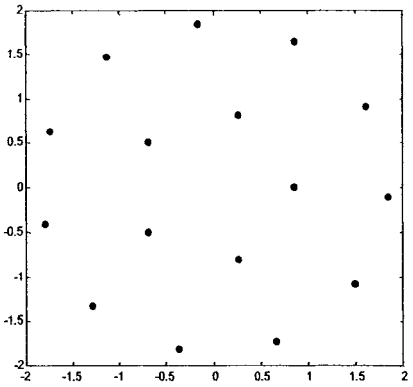

Fig. 5.7: (11,5)APK constellation

Constellation set	$\bar{P}_{ave}$(dB)	PAR (dB)	W(dB)
Square 16QAM	3.98	2.55	6.53
circular (11,5)APK	4.11	1.23	5.34

Table 5.2: Performance comparison between square 16QAM and circular (11,5)APK

The exact symbol error rate versus signal to noise ratio curves (Figure 5.8) show that the (11,5)APK has a slightly better performance of around 0.12dB as compared to the square 16QAM. Based on the simulation results, the overall advantage of the (11,5)APK over the square 16QAM is about 1.44 dB.

One disadvantage of the circular M-APK constellation is that it requires higher complexity at the demodulator comparing with that of square M-QAM constellation. For the case of square M-QAM, the inphase and quadrature phase of a signal can be demodulated independently, and it is very simple to implement the detector. However, this cannot be done for circular M-APK, since the shapes of the decision boundary are not rectangle and more complicated. Because the points on the circular M-APK constellation vary both amplitude and phase, it would be simpler to implement the

detector in polar format. In other words, a signal is converted from IQ to polar format and then fed to the detector. Basing on the amplitude and phase of the received signal, the detector will make the decision on which region the received signal falling in and therefore the closest point on the constellation.

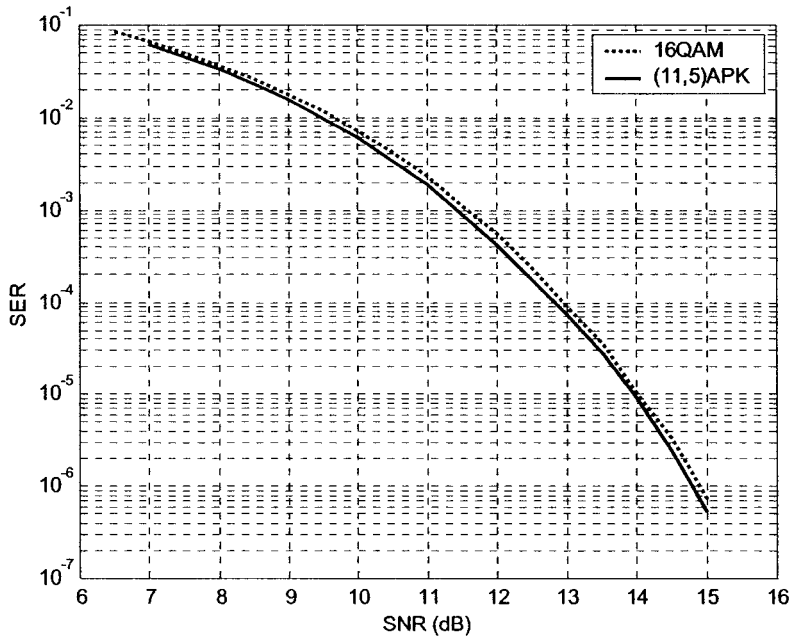

Fig. 5.8: Symbol error rate of square 16QAM and (11,5)APK

5.5.3. Circular (17,10,5)APK

Figure 5.10 depicts the optimal (17,10,5)APK constellation for M=32 with 17, 10, and 5 elements on the outer, middle, and inner circles, respectively. Its performance is compared to that of the popular cross 32QAM (Figure 5.9). The cross constellation shape can provide low PAR. The results summarized in Table 5.3 indicate that the (17,10,5)APK has higher normalized average power and slightly lower peak to average power ratio than the cross 32QAM. The overall gain of the (17,10,5)APK is only 0.44 dB as compared to the cross 32QAM.

Exact SER curves plotted in Figure 5.11 show that the (17,10,5)APK and cross

32QAM have almost the same performance although their normalized average power difference is about 0.13dB. Based on the simulation results, the overall advantage of the (17,10,5)APK over the cross 32QAM is about 0.58dB.

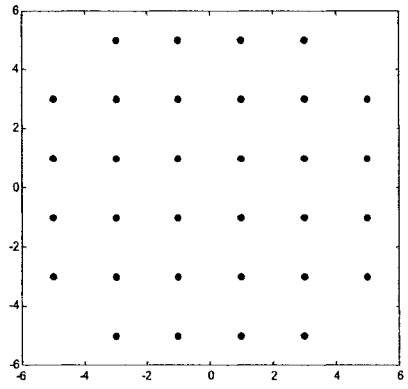

Fig. 5.9: Cross 32QAM constellation

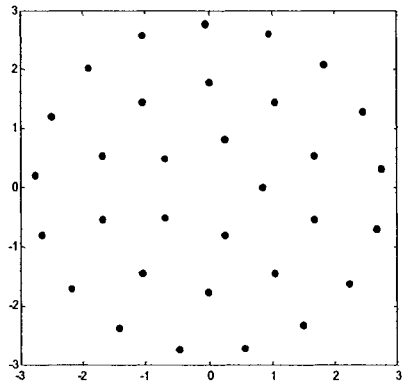

Fig. 5.10: (17,10,5)APK constellation

Constellation set	$\bar{P}_{ave}$(dB)	PAR (dB)	W(dB)
Cross 32QAM	6.99	2.30	9.29
(17,10,5)APK	7.14	1.71	8.85

Table 5.3: Performance comparison between cross 32QAM and (17,10,5)APK

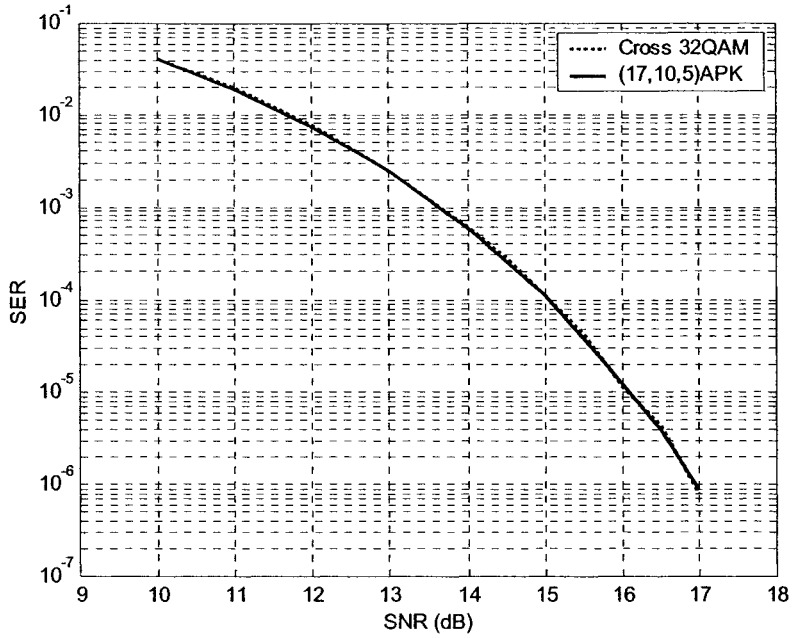

Fig. 5.11: Symbol error rate of cross 32QAM and (17,10,5)APK

5.5.4. Circular (25,19,13,6,1)APK

The obtained optimum constellation for M=64 is the (25,19,13,6,1)APK shown in Figure 5.13. Table 5.4 compares the normalized average power and peak to average power ratio of (25,19,13,6,1)APK and square 64QAM (Figure 5.12). The (25,19,13,6,1)APK has slightly lower $\bar{P}_{ave}$ and much lower PAR than the square 64QAM with an overall gain of 1.66dB. The exact symbol error rate curves plotted in Figure 5.14 indicate that the (25,19,13,6,1)APK outperforms the square 64QAM by 0.2dB. Taking into account the PAR, the overall advantage of the (25,19,13,6,1)APK over the square 64QAM is about 1.79dB.

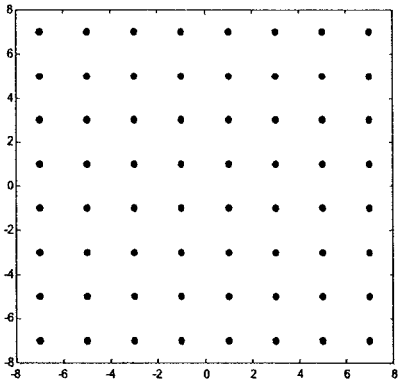

Fig. 5.12: Square 64QAM constellation

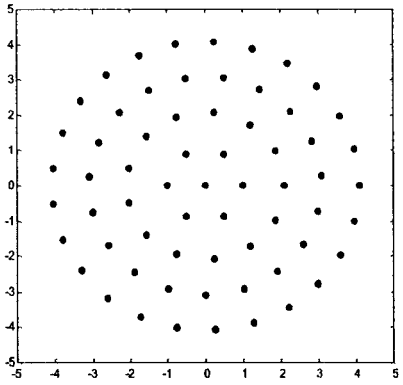

Fig. 5.13: (25,19,13,6,1)APK constellation

Constellation set	$\bar{P}_{ave}$(dB)	PAR (dB)	W(dB)
Square 64QAM	10.21	3.68	13.89
(25,19,13,6,1) APK	10.14	2.09	12.23

Table 5.4: Performance comparison between square 64QAM and (25,19,13,6,1)APK

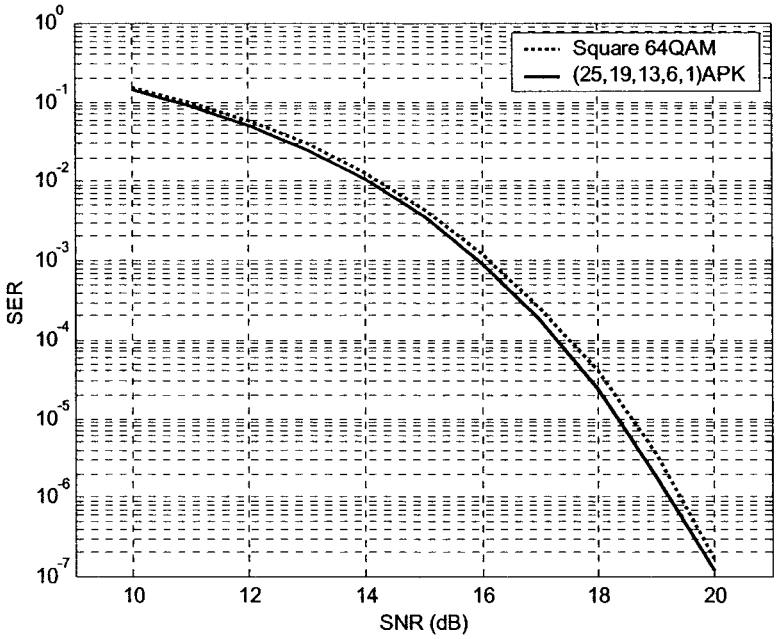

Fig. 5.14: Symbol error rate of square 64QAM and (25,19,13,6,1)APK

5.5.5. Circular (37,30,24,18,12,6,1)APK

For M=128, the search results in the optimal (37,30,24,18,12,6,1)APK constellation with one element at the center and others located on six circles as shown in Figure 5.16. The popular cross 128QAM (Figure 5.15) is used for performance comparison. The results summarized in Table 5.5 show that the performance of the (37,30,24,18,12,6,1)APK is better than that of the cross 128-QAM by about 0.87dB. The exact SER curves (Figure 5.17) indicate that the (37,30,24,18,12,6,1)APK has a better performance than the cross 128QAM by about 0.18dB. This provides an overall advantage of the (37,30,24,18,12,6,1)APK over the cross 128QAM of about 0.97dB.

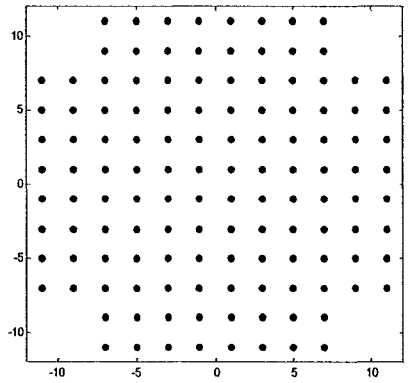

Fig. 5.15: Cross 128QAM constellation

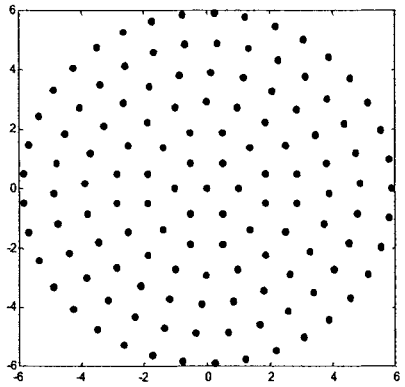

Fig. 5.16: (37,30,24,18,12,6,1)APK constellation

Constellation set	$\overline{P}_{ave}$(dB)	PAR (dB)	W(dB)
Cross 128QAM	13.11	3.17	16.28
(37,30,24,18,12,6,1)APK	13.03	2.38	15.41

Table 5.5: Performance comparison between cross 128QAM and (37,30,24,18,12,6,1)APK

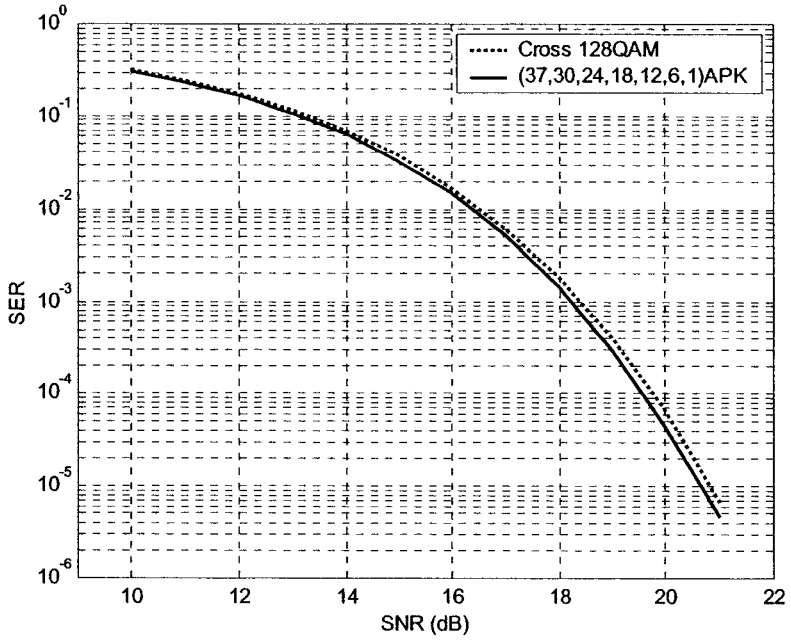

Fig. 5.17: Symbol error rate of cross 128QAM and (37,30,24,18,12,6,1)APK

Chapter 6. Conclusions

In this thesis, polynomial predistorters based on polar structure suitable for M-QAM systems using nonlinear power amplifier are presented. For adaptive algorithms, we developed both LMS-based and RLS-based algorithms. The LMS adaptive structure has low complexity and slow convergence rate. A faster LMS-based algorithm can be achieved with an increase in complexity. However, for applications requiring a very fast convergence rate, RLS-based algorithms are the better choices. We proposed a cascaded adaptive predistorter structure for further enhanced convergence rates.

The analysis of quantization effects indicates that a wordlength of 9 bits to represent the coefficients of the amplitude and phase predistorter polynomials and the lookup table can provide a performance close to that in the case of floating-point computation. The equivalent predistorter-amplifier operating at low PBO can offer both performance and transmitted spectrum similar to the ideal linear case.

Both analytical and simulation results indicate good transient and steady-state performance. They show that power amplifiers can operate with the peak power backoff (PBO) of 0.22dB (i.e., near saturation) while the bandlimited M-ary QAM signals can preserve the same spectra and BER performance as in a linear channel. The average output power backoff (OBO) depends on the peak-to-average power ratio (PAR) of the modulated signal. For further increase in power efficiency of the transmitter, OBO can be reduced with low-PAR modulated signal.

The overall PAR of a modulated signal was shown to have two parts: one due to the sharpness or the roll-off factor of the spectrum shaping filter, and the other is related to the designed constellation. This gave the motivation to search for bandwidth-efficient multilevel modulation schemes with good performance in AWGN and suitable for

transmitters using nonlinear power amplifiers. We focus on modulated signals with circular constellations and aim to minimize their PAR and to maximize their squared-minimum-distance-to-average-power ratio (DPR).

A search algorithm based on two criteria, DPR and PAR, was proposed to find the optimum circular constellations M-APK signalling schemes suitable for non-linear amplification. The results showed that the sets (7,1), (11,7), (17,10,5), (25,19,13,6,1), (37,30,24,18,12,6,1) are the optimal sets for 8-,16-,32-,64-,128-APK constellations respectively. They were verified by simulation and by comparing the SNR of the optimal APK constellations with the popular M-ary QAM constellations. Both analytical and simulation results showed that the optimal APK constellations outperform the cross, rectangular M-ary QAM constellations. It suggests that these optimal APK sets can be used to improve the performance of a system using non-linear power amplifiers to achieve high power efficiency.

Further works could be carried out to study the performance and complexity of a predistorter scheme that combines the polynomial and lookup table techniques. When the lookup table size increases, the order of the polynomial decreases and vice versa. It is expected that given power amplifier characteristics, there will be optimal values of the polynomial order and the table size such that it gives the best performance and low complexity.

Trellis-coded modulation schemes specifically designed to operate on fading channels have shown great potential. Bandwith-efficient modulations with operate effectively in the presence of fading are of particular interest for mobile communications systems. The further study of the work reported in this thesis and trellis-coded scheme may improve the system performance. The following subjects can be carried out for further studies:

a) Trellis-coded schemes with low-PAR circular APK constellations.

b) Combined predistortion and trellis-coded schemes with low-PAR circular APK constellations.

References

[1] E. G. Jeckeln, F M. Ghannouchi, and M. Sawan, "Adaptive digital predistorter for power amplifiers with real time modeling of memoryless complex gains" *Proceeding of IEEE MTT-S Digest*, pp. 835-838, 1996

[2] R. Stewart and F. Tusubira, "Feedforward linearization of 950 MHz Amplifiers", *IEE Proceedings*, Vol. 135, pp. 347-350, Oct. 1988.

[3] M.A. Briffa and M. Faulkner, "Stability analysis of Cartesian feedback linearisation for amplifiers with weak nonlinearities", *IEE Proceedings- Communications*, Vol. 143, No. 4 , pp. 212 -218, Aug. 1996.

[4] J. K. Cavers, "Adaptation behavior of a feedforward amplifier linearizer", *IEEE Trans. on Veh. Tech.*, Vol. 44, No. 1, pp. 31-40, Feb. 1995

[5] A. A. M. Saleh and J. Salz, "Adaptive linearization of power amplifiers in digital radio systems", *The Bell System Technical Journal*, Vol. 62, No. 4, pp. 1019-1033, April 1983.

[6] Y. Nagata, "Linear amplification technique for digital mobile communications", *In Proceedings of IEEE Vehicular Technology Conference VTC'89*, Vol. 1, pp. 159-164, San Francisco 1989.

[7] J. Namiki, "An automatically controlled predistorter for multilevel quadrature amplitude modulation", *IEEE Trans. Commun.*, Vol. 31, No. 5., pp 707-712 May.1983.

[8] G. Karam and H. Sari, "Analysis of predistortion, equalization, and ISI cancellation techniques in digital radio systems with non-linear transmit amplifiers", *IEEE Trans. Commun.*, Vol. 37, No. 12, pp. 1245-1253, Dec. 1989.

[9] G. Karam and H. Sari, "A data predistortion technique with memory for QAM radio systems", *IEEE Trans. Commun.*, Vol. 39, No. 2, pp. 336-344, Feb. 1991.

[10] S. Benedetto, E. Biglieri, and V. Castellani, *Digital Transmission Theory*, Prentice-Hall, 1987.

[11] C. Eun and E. J. Powers, "A new Volterra predistorter based on the indirect learning architecture", *IEEE Trans. Signal Processing*, Vol. 45, No. 1, pp. 223-227, Jan. 1997.

[12] N. Benvenuto, F. Piazza , and A. Uncini, "A neural network approach to data predistortion with memory in digital radio systems", *Proceeding of IEEE International Conference on Communications*, pp. 232-236, Geneva, Switzerland, 1993.

[13] C. H. and E. J. Powers, "A reconsideration of the pth-order inverse predistorter", *Proceedings of 49th IEEE Vehicular Technology Conference VTC'99*, Vol. 2, pp. 1501-1504, 1999.

[14] H. W. Kang, Y. S. Cho, and D. H. Youn, "On compensating nonlinear distortions of an OFDM system using an efficient adaptive predistorter", *IEEE Trans. Commun.*, Vol. 47, No. 4., pp. 522-526 April 1999.

[15] J. K. Cavers, "Amplifier linearization using a digital predistorter with fast adaptation and low memory requirements", *IEEE Trans. Veh. Tech.*, Vol. 39, No. 4, pp. 374-382, Nov.1990.

[16] J. K. Cavers, "New methods for adaptation of quadrature modulators and demodulators in amplifier linearization circuits", *IEEE Trans. Veh. Tech.*, Vol. 46, No. 3, pp. 707-716, Aug. 1997.

[17] J. K. Cavers, "Optimum table spacing in predistorting amplifier linearizers", *IEEE Trans. Veh. Tech.*, Vol. 48, No. 5, pp. 1699-1705, Sep. 1999.

[18] M. Faulkner and M. Johansson, "Adaptive linearization using predistortion, experimental results", *IEEE Trans. Veh. Tech.*, Vol. 43, No2, pp. 323-332, May. 1994.

[19] A. S. Wright and W. G. Durtler, "Experimental performance of an adaptive digital linearized power amplifier", *IEEE Trans. Veh. Tech.*, Vol. 41, No. 4, Nov. 1992

[20] S. P. Stapleton, G. S. Kandola, and J. K. Cavers, "Simulation and analysis of an adaptive predistorter utilizing a complex spectral convolution", *IEEE Trans. Veh. Tech.*, Vol. 41, No4, pp. 387-394, Nov. 1992.

[21] M. Ghaderi, S. Kumar, and D. E. Dodds, "Adaptive predistortion lineariser using polynomial functions", *IEE Proc. Commun.*, Vol. 141, No. 2, pp. 49-55, April 1994.

[22] M. Ghaderi, S. Kumar, and D. E. Dodds, "Fast adaptive polynomial I and Q predistorter with global optimisation", *IEE Proc. Commun.*, Vol. 143, No. 2, pp. 78-86, April 1996.

[23] A. N. D'Andrea, V. Lottici, and R. Reggiannini, "RF power amplifier linearization through amplitude and phase predistortion", *IEEE Trans. Commun.*, Vol. 44, No. 11, pp. 1477-1484, Nov. 1996.

[24] B. Hichem, T. Le-Ngoc "A fast adaptive predistorter for nonlinearity amplified M-QAM signal", *Global Telecommunications Conference*, Vol 1, pp. 108 -112, 2000.

[25] John G. Proakis, *Digital communications*, McGraw-Hill, 3rd ed, 1995.

[26] A. S. Sedra and K. C. Smith, *Microelectronic circuits*, Oxford University Press Inc., 3rd ed., 1991.

[27] L. Sundstrom, *Digital RF Power Amplifier Linearisers. Analysis and Design*. Ph.D dissertation, Lund university, sweden, August 1995.

[28] D. E. Johnson, *Adaptive Digital Predistortion With Applications for LMDS Systems*. M.S. Thesis, Virginia Polytech Institute and State University, USA, August 2000.

[29] A. A. Saleh, "Frequency-independent and frequency-dependent nonlinear models of TWT amplifiers", *IEEE Trans. Commun.*, Vol 29, No 11, pp 1715-1720, Nov. 1981.

[30] J. L. Fikart, B. Kocay, "Cost effective operating power specification of Ka-Band MMICs for multimedia satellite interactive terminals", *Proc. 1999 IEEE MTT-S International Topical Symposium on Technologies for Wireless Applications*, pp: 247 -252, 1999

[31] Y.H. Hu, "The quantization effects of the CORDIC algorithm", *IEEE Trans. Signal Processing*, Vol. 45, pp. 834 -844, April 1992.

[32] L. Sundstrom, "Quantization analysis and design of a digital predistortion linearizer for RF power amplifier", *IEEE Trans. Veh. Tech.*, Vol. 45, No. 4, pp. 707-719, Nov. 1996.

[33] S. Haykin, *Adaptive Filter Theory,* Prentice-Hall editor, 3rd ed., 1996.

[34] R. H. Kwong and E. W. Johnston, "A variable step size LMS algorithm", *IEEE Trans. Signal Processing.*, Vol. 40, No. 7, pp. 1633-1642, July 1992.

[35] C. F. N. Cowan, "Performance comparisons of finite linear adaptive filters", *IEE Proceedings*, Vol. 134, pp. 211-216, 1987.

[36] B. W. Kernighan and S. Lin, "Heuristic solution of a signal design optimization problem", *The Bell System Technical Journal* , Vol. 52, No. 7, pp. 1145-1159, Sep. 1973.

[37] C. Melvil Thomas, Michael Y. Weidner, and S. H. Durrani, "Digital amplitude-phase keying with m-ary alphabets", *IEEE Trans. Commun.*, Vol. 22, No. 2, pp. 168-179, Feb. 1974.

[38] Yugang Zhou and Peter J. McLane, "Simple predistortion method for higher order APK modulation for a nonliear power amplifier channel", *CITR report*, 2000.

[39] Xiaodai Dong, Norman C. Beaulieu, and Paul H. Wittke, "Signaling constellations for fading channels", *IEEE Trans. Commun.*, Vol. 47, No. 5, pp. 703-714, May. 1999.

[40] R. Blyth and E. V. Jones, "Signal constellations based on hypercubes", *IEE Conference on Telecommunications*, pp. 83-87, 1994.

[41] Zoran H. Peric et al., "Design of signal constellations for gaussian channel by using iterative polar quantization", *Mediterranean Electrotechnical Conference*, Vol. 2 , pp. 866-869, 1998.

[42] Anand G. Dabak, "Signal constellations for non-Gaussian communication problems", *IEEE International Conference on Acoustics, Speech, and Signal Processing*, Vol. 3 , pp. 33-36, 1993.